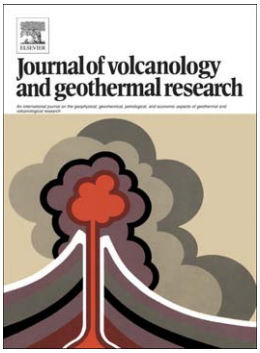

Geochemistry of the Late Holocene rocks from the Tolbachik volcanic field, Kamchatka: Quantitative modelling of subduction-related open magmatic systems

Maxim Portnyagin, Svend Duggen, Folkmar Hauff, Nikita Mironov, Ilya Bindeman, Matthew Thirlwall, Kaj Hoernle

PII: S0377-0273(15)00271-1
DOI: doi: 10.1016/j.jvolgeores.2015.08.015
Reference: VOLGEO 5632

To appear in: *Journal of Volcanology and Geothermal Research*

Received date: 14 February 2015
Accepted date: 14 August 2015

Please cite this article as: Portnyagin, Maxim, Duggen, Svend, Hauff, Folkmar, Mironov, Nikita, Bindeman, Ilya, Thirlwall, Matthew, Hoernle, Kaj, Geochemistry of the Late Holocene rocks from the Tolbachik volcanic field, Kamchatka: Quantitative modelling of subduction-related open magmatic systems, *Journal of Volcanology and Geothermal Research* (2015), doi: 10.1016/j.jvolgeores.2015.08.015

Geochemistry of the Late Holocene rocks from the Tolbachik volcanic field, Kamchatka: Quantitative modelling of subduction-related open magmatic systems

Maxim Portnyagin[1,2*], Svend Duggen[1,3,4], Folkmar Hauff[1],

Nikita Mironov[2], Ilya Bindeman[5], Matthew Thirlwall[3], Kaj Hoernle[1,6]

[1] GEOMAR Helmholtz Centre for Ocean Research Kiel, Wischhofstrasse 1-3, 24148 Kiel, Germany

[2] V.I. Vernadsky Institute of Geochemistry and Analytical Chemistry, Kosygin str. 19, Moscow, 119991, Russia

[3] Department of Geology, Royal Holloway University of London, Egham, Surrey TW20 OEX, United Kingdom.

[4] A.P. Møller Skolen, Fjordallee 1, 24837 Schleswig, Germany

[5] Geological Sciences, 1272 University of Oregon, Eugene, OR 97403, USA

[6] Christian Albrechts University of Kiel, Kiel, Germany

*Corresponding author: mportnyagin@geomar.de, tel. +49 (0)431 600 2636

Highlights:

- New geochemical data for the Tolbachik lava field including 2012-2013 eruption
- Tolbachik rocks exhibit small isotopic but large trace element variability
- A quantitative model for the origin of primary Tolbachik magma is presented
- Fractional crystallization ± assimilation cannot alone explain Tolbachik chemistry
- Fractionation occurred in a periodically replenished and evacuated magma chamber

Key words:

subduction zone, Kamchatka, Tolbachik, mantle wedge, slab component, primary magma, REFC, chalcophile elements

Abstract

We present new major and trace element, high-precision Sr-Nd-Pb (double spike), and O-isotope data for the whole range of rocks from the Holocene Tolbachik volcanic field in the Central Kamchatka Depression (CKD). The Tolbachik rocks range from high-Mg basalts to low-Mg basaltic trachyandesites. The rocks considered in this paper represent mostly Late Holocene eruptions (using tephrochronological dating), including historic ones in 1941, 1975-1976 and 2012-2013. Major compositional features of the Tolbachik volcanic rocks include the prolonged predominance of one erupted magma type, close association of middle-K primitive and high-K evolved rocks, large variations in incompatible element abundances and ratios but narrow range in isotopic composition. We quantify the conditions of the Tolbachik magma origin and evolution and revise previously proposed models. We conclude that all Tolbachik rocks are genetically related by crystal fractionation of medium-K primary magmas with only a small range in trace element and isotope composition. The primary Tolbachik magmas contain ~14 wt% MgO and ~4% wt% H_2O and originated by partial melting (~6%) of moderately depleted mantle peridotite with Indian-MORB-type isotopic composition at temperature of ~1250^{o}C and pressure of ~2 GPa. The melting of the mantle wedge was triggered by slab-derived hydrous melts formed at ~2.8 GPa and ~725^{o}C from a mixture of sediments and MORB- and Meiji- type altered oceanic crust. The primary magmas experienced a complex open-system evolution termed Recharge-Evacuation-Fractional Crystallization (REFC). First the original primary magmas underwent open-system crystal fractionation combined with periodic recharge of the magma chamber with more primitive magma, followed by mixing of both magma types, further fractionation and finally eruption.

Evolved high-K basalts, which predominate in the Tolbachik field, and basaltic trachyandesites erupted in 2012-2013 approach steady-state REFC liquid compositions at different eruption or replenishment rates. Intermediate rocks, including high-K, high-Mg basalts, are formed by mixing of the evolved and primitive magmas. Evolution of Tolbachik magmas is associated with large fractionation between incompatible trace elements (e.g., Rb/Ba, La/Nb, Ba/Th) and is strongly controlled by the relative difference in partitioning between crystal and liquid phases. The Tolbachik volcanic field shows that open-system scenarios provide more plausible and precise descriptions of long-lived arc magmatic systems than simpler, but often geologically unrealistic, closed-system models.

1. Introduction

The Tolbachik volcanic field is the largest and most active area of predominantly basaltic monogenetic volcanism in Kamchatka (Ponomareva et al., 2007). Spectacular eruptions, erupting large volumes of lava for several months, can be studied in great detail due to the predominantly effusive character of the eruptions and relatively easy access (Fedotov and Markhinin, 1991; Belousov et al., 2015).

The Tolbachik volcanic series primarily comprises two rock types: middle-K, high-Mg (high-MgO/Al_2O_3) basalts (HMB) and high-K, high-Al (low-MgO/Al_2O_3) basalts (HAB) (Flerov and Bogayavlenskaya, 1983; Braitseva et al., 1983). HAB were erupted during all volcanic episodes in the Tolbachik volcanic field. HMB have only been erupted during the last ~ 2ka and generally preceded HAB eruptions. During the Great Fissure Tolbachik eruption (GFTE) in 1975-1976 (Volynets et al., 1983), for example, the two lava types erupted sequentially from closely spaced vents. Small volumes of magmas of intermediate composition between HMB and HAB were erupted in the final and early stages of the Northern and Southern GFTE vents, respectively.

The Tolbachik rock series can provide key insights into the origin and evolution of subduction-related magmas for at least two reasons. First, crystal-poor, high-magnesian Tolbachik basalts are among the most primitive arc rocks globally (Portnyagin et al., 2007a), which represent near primary arc magmas and can be used to reconstruct the conditions of their generation with minimal extrapolation. The conditions of the Tolbachik primary magma generation have not been quantified in detail thus far. Second, genetic relationships between the two major Tolbachik rock types remain unresolved. Particularly controversial is the origin of high-K HAB, which cannot be related to middle-K HMB by simple fractional crystallization (e.g., Volynets et al., 1983;

Churikova et al., 2001; Dosetto et al., 2003), even though fractional crystallization is widely accepted for the origin of most HAB in Kamchatka (Ariskin et al., 1995; Kersting and Arculus, 1994; Ozerov, 2000; Volynets, 1994) and worldwide (Meyers and Johnston, 1996). In 2012-2013 the latest Tolbachik eruption produced more evolved lavas (high-K basaltic trachyandesites) compared to all previously reported compositions from the Tolbachik area (Volynets et al., 2013; 2015), re-awakening interest in the genetic relationships within the entire Tolbachik rocks series.

In this study we use new high-quality geochemical data (major and trace elements, Sr-Nd-Pb-O isotopes) and computational petrological tools and models to decipher the composition and origin of primary Tolbachik magmas, the genetic relationships between different types of recent Tolbachik magmas, and the temporal evolution of the volcanic system. This discussion is reinforced by the new information obtained on magmas erupted in 2012-2013. Our study contributes to improving the understanding of the origin of volcanism in Kamchatka, and subduction-related settings in general, and re-emphasizes the necessity to apply open-system geochemical models in studies aimed at deciphering and modelling the evolution and compositional features of long-lived subduction-related volcanoes and volcanic fields.

2. Geological background and studied rocks

The Kamchatka Peninsula located in the Russian Far East is one of the most active volcanic areas on Earth (Fig. 1). Volcanism in Kamchatka is related to subduction of Mesozoic Pacific lithosphere, including the Hawaiian-Emperor Seamount chain, at a speed of ~75 km/Ma (Syracuse and Abers, 2006). Based on seismic data, the slab dip

angle progressively decreases northward from Tolbachik (~45°) to Shiveluch (~25°) volcano (Gorbatov et al., 1997), possibly resulting from the subduction of the Hawaiian-Emperor hotspot track or increasing proximity to the Aleutian Arc. Subduction of the seamount chain and/or proximity to the Aleutian Arc may also be responsible for the westward displacement of volcanic activity from the Eastern volcanic belt (EVF) to the Central Kamchatkan Depression (CKD) (Fig. 1). Crustal thickness is fairly constant throughout the CKD (~30-35 km), similar to most other parts of Kamchatka (Balesta, 1981; Levin et al., 2002), arguing against crustal thinning under the CKD unless massive underplating with basaltic material has also taken place (Balesta, 1981).

Late Pleistocene to Holocene volcanoes of the Klyuchevskaya group (e.g. Klyuchevskoy, Bezymianny, Kamen and Tolbachik), built on a massive Pleistocene basaltic plateau, are also located in the CKD (Fig. 1). Plosky Tolbachik, its predecessor Ostry Tolbachik and an associated field of monogenetic cinder cones and lavas, the Tolbachik volcanic field, are the southernmost active volcanoes in CKD.

Detailed geological information of the Tolbachik volcanic field can be found in a book devoted to the Great Tolbachik Fissure eruption (Fedotov and Markhinin, 1983). In brief, the volcanic field covers an area of 875 km^2. It is associated with a regional fissure swarm and consists of numerous cinder cones and associated lava flows (Fig. 1). The fissure zone extends for ~50 km, from the southern end of the Tolbachik field through the Plosky Tolbachik volcano edifice and extends for another ~14 km to the northeast.

On the basis of tephrochronological dating, two major periods of volcanic activity were recognised in the Tolbachik field (Braitseva et al., 1983): (I) from ~10 to 1.7 ka, and (II) from 1.7 ka to present (here we use updated calibrated ^{14}C ages following Churikova

et al., this volume). Summarizing the data of Braitseva et al. (1983), Period I was predominantly effusive with a lava/tephra mass ratio of ~7.5. The total mass of erupted magmas is estimated to amount 125×10^9 t with an average productivity of 18×10^6 t/y. The magmas were predominantly (>90%) high-K HABs with $MgO/Al_2O_3<0.4$. More magnesian basalts were present in very subordinate amounts. Period II is characterized by the arrival of abundant HMB with $MgO/Al_2O_3>0.6$ and also transitional basalts between HAB and HMB, which also preceded eruption of HAB during several eruptions (e.g., GFTE and Alaid cone). Period II eruptions were more explosive with a lava/tephra ratio of ~2.7. The total mass of erupted magma was estimated at $\sim48\times10^9$ t with an average magma flux of $\sim28\times10^6$ t/y. The average amount of erupted HAB appears to have decreased from ~20 to 10×10^6 t/y during Period II, whereas the amount of HMB and transitional basalts erupted has varied significantly with an average output rate of $\sim10\times10^6$ t/y.

Period I volcanic activity in the Tolbachik field is represented by only one sample in our collection (K01-49, Table 1). This rock was collected from a geologically complex area of presumably 1.7-7.8 ka lavas surrounded by younger lava flows. The geochemical peculiarity of this sample (see below) makes us confident that our interpretation of the sample age is correct. All other samples studied here represent Period II activity in the Tolbachik volcanic field, including historic eruptions of 1941, 1975-1976 and 2012-2013. The samples were collected in 2001 from cinder cones (volcanic bombs) and associated lava flows along the axial part of the volcanic field (Fig. 1). Some samples were collected from the area now covered with lava and tephra from the 2012-2013 eruption (e.g., Krasny cone). Products of the 2012-2013 eruption are represented by fine (< 1mm) ash of

the initial explosive activity on 27/11/2012. These samples were collected 5 cm below the snow surface 54 km NNW of the vent near Maiskoe village a few days after the onset of the eruption and were generously provided by Dmitri Melnikov. Lapilli ejected from the second vent on 25/02/2013 and a sample collected from an advancing lava front on 02/03/2013 were generously provided by Dmitri Saveliev.

In addition we studied three basaltic xenoliths found in pyroclastic rocks from the 1975 eruption (cones II and III) and the Peschanie Gorki cone (0.7-1.4 ka) and one sample (K01-65) of mega-plagioclase-phyric basalt from the Pleistocene pedestal of the Klyuchevskoy group of volcanoes, collected from the Kamchatka River coastal bank in Kozyrevsk village. Geographic coordinates, rock types and a general description of the samples are reported in Table 1.

3. Methods and analytical techniques

For major and trace element analysis, fresh parts of the samples were crushed in a steel jaw crusher and powdered in agate mills. Most bulk rock analyses were performed on fused beads with a Philips X´unique PW 1480 X-ray flourescence spectrometer (XRF) at the Leibniz-Institute of Marine Sciences IFM-GEOMAR in Kiel (now GEOMAR Helmholtz Centre for Ocean Research Kiel), Germany. CO_2 and H_2O were determined with a Rosemont Infrared Photometer CSA 5003. Samples from the 2012-13 eruption were analysed by XRF on fused pellets using a Magix Pro PW 2540 XRF at the Institute of Mineralogy and Petrography at the University of Hamburg, Germany. In both labs international reference samples JB-2, JB-3, JA-2, JA-3, JR-2, JR-3, JG-2 provided by the Geological Survey of Japan (https://gbank.gsj.jp/geostandards/gsj1mainj.html) were

measured along with the samples. The accuracy and precision were within the reference values compiled in GeoReM (http://georem.mpch-mainz.gwdg.de/) (Table A1).

Selected trace elements (Ni, Cr, V, Sc, Cu, Zn, Cl, Ga, Pb, Sr, Rb, Ba, Zr, Nb, Th, Y, La, Ce and Nd) were analysed on pressed pellets using the Philips PW 1480 XRF spectrometer at the Department of Geology, Royal Holloway College, University of London (RHUL). The calibration was based on up to 40 international standard samples and matrix corrections were performed based on the major element composition. Each sample was measured three times alternating with a standard and the average concentrations and standard deviations are reported in Table 2. Typical reproducibility and accuracy of repeat analyses of standard samples is on the order of 1 rel. % for most elements and 0.3 ppm for Pb, Th, Y, 1.5-2 ppm for La, Ce and Nd and 5 rel. % for Cl (Thirlwall, 2000) (Table A1).

Three samples were analysed for an extended range of trace elements by solution inductively coupled plasma mass spectrometry (ICP-MS) at the Institute of Geoscience, University of Kiel. Trace elements were determined from mixed acid (HF-aqua regia-$HClO_4$) pressure digests by using an Agilent 7500cs ICP-MS instrument (Garbe-Schönberg, 1993; Portnyagin et al., 2005). The precision was better than 3 % RSD (relative standard deviation) as estimated from duplicate measurements. Blanks and international standards, AGV-1 and BHVO-1 provided by the United States Geological Survey (USSGS) (http://crustal.usgs.gov/geochemical_reference_standards/index.html), were digested and analysed in one series with the samples in order to evaluate the precision and accuracy of the measurements. The data on standard measurements are reported in Table A2.

Electron microprobe (EMP) analyses of glass shards from pyroclastic rocks of the 2012-2013 eruption were obtained at GEOMAR following the routine established for tephra glass analysis at GEOMAR (Ponomareva et al., 2013).

Sr- and Nd-isotope analyses of the pre-2012 rocks were performed at RHUL using the VG354 multi-collector thermal ionisation mass spectrometer (TIMS). Chemical procedures were performed in Class 10,000 clean laboratories. For Sr-isotope analysis, the whole rock powders were leached prior to dissolution in polytetraflouroethylene (PTFE) Savillex beakers with 6 M HCl on a hotplate for one hour and then rinsed with ultrapure water. For both Sr- and Nd-isotope analysis, the whole rock powders were dissolved in separate Savillex beakers with a concentrated HNO_3-HF mixture on a hotplate. After dissolution and conversion to nitrate, Sr was separated from the matrix elements of the leached batch and purified with two passes through the Sr-Spec extraction resin loaded into small pipette-tip sized columns. The light rare earth elements were separated from the matrix elements in the second, unleached batch on small columns filled with ~50 mg of TRU-Spec resin and subsequently Nd was separated from the other rare earth elements by two passes on cation exchange columns. The Sr was loaded on single Re-filaments using the TaF_5 sandwich-loading technique and Sr-isotope ratios were measured multi-dynamically. Nd was run multi-dynamically as NdO^+ after loading on single Re-filaments with dilute H_3PO_4 and silica gel. Further details of the analytical procedures are reported in the literature (Thirlwall, 1991a; Thirlwall, 1991b). Sample data are reported relative to $^{87}Sr/^{86}Sr = 0.710248 \pm 0.000014$ (n=12, 2σ) for NIST SRM987 and $^{143}Nd/^{144}Nd = 0.511856 \pm 0.000006$ (n=10, 2σ) for La Jolla. The Sr-Nd-isotope data along with internal errors (2σ) are reported in Table 4.

The Pb double spike isotope analysis was performed in the ultraclean laboratories at RHUL using Class 100 Picotrace clean hoods and an Isoprobe multicollector-inductively coupled plasma-mass spectrometer (MC-ICP-MS). Pb-isotope analysis was performed on whole rock chips (0.5-1 mm) that were handpicked under the binocular microscope. The chips (~100 mg) were acid washed with 6M HCl in cleaned Savillex beakers at 150° C on a hotplate and multiply rinsed with 18.2 MΩ water and then digested ~24 hours with a few millilitres of an HNO_3-HF acid mixture at 150° C. The beakers, water and acids were Pb-blank tested prior to use. Details on the analytical procedures involving MC-ICP-MS analysis and data reduction (e.g. corrections for instrument memory, peak tailing, isobaric interferences and mass bias using the double spike and exponential law) are given in the literature (Thirlwall, 2000). NIST SRM981, treated as an unknown and normalised to NIST SRM982 $^{208}Pb/^{206}Pb$ = 1.00016, gave ratios of $^{206}Pb/^{204}Pb$ = 16.9384 (0.0018, 2σ), $^{207}Pb/^{204}Pb$ = 15.4966 (0.0018, 2σ) and $^{208}Pb/^{204}Pb$ = 36.7157 (0.0051, 2σ) during the course of this study (n = 12), consistent with data presented by (Thirlwall, 2000). The Pb double spike isotope data and standard errors (2SE) are reported in Table 4.

From the 2012-2013 eruption, 0.5-2mm sized chips of samples were analyzed at GEOMAR Helmholtz Centre for Ocean Research Kiel for Sr-Nd-Pb isotopic composition. About 150-300 mg of sample material was leached in ultrapure 2N HCl at 70˚C for 1h and then triple rinsed with ultrapure water. Sample dissolution uses a HF-HNO_3 mixture at 150°C for 48 hours in closed 15ml Teflon beakers followed by sequential, standard ion exchange procedure of (Hoernle et al., 2008) to separate Pb, Sr and Nd from the sample matrix. Sr and Nd isotope ratios were determined on a

ThermoFinnigan TRITON thermal ionization mass spectrometer (TIMS) and Pb on a Finnigan MAT262 RPQ^{2+} TIMS. Both instruments operate in static multi-collection mode with Sr and Nd being normalized within run to $^{86}Sr/^{88}Sr = 0.1194$ and $^{146}Nd/^{144}Nd = 0.7219$ respectively. Sample data are reported relative to $^{87}Sr/^{86}Sr = 0.710250 \pm 0.000007$ (n=6, 2σ) for NIST SRM987 and $^{143}Nd/^{144}Nd = 0.511850 \pm 0.000011$ (n=5, 2σ) for La Jolla. Pb mass bias correction follows the Pb double spike (DS) technique of (Hoernle et al., 2011). In the period 2012-2014, DS corrected NIST SRM981 gave $^{206}Pb/^{204}Pb = 16.9417 \pm 0.00027$, $^{207}Pb/^{204}Pb = 15.4991 \pm 0.0027$, $^{208}Pb/^{204}Pb = 36.7249 \pm 0.0070$, $^{207}Pb/^{206}Pb = 0.91485 \pm 0.00004$ and $^{208}Pb/^{206}Pb = 2.16772 \pm 0.00013$ (n=95, 2σ). These values compare well with published double and triple spike data for NIST SRM981(Baker et al., 2004; Baker et al., 2005; Galer, 1999; Thirlwall, 2000). To allow unbiased comparison of sample data the RUHL NIST SRM981 DS (MC-ICPMS) values were divided by the GEOMAR NIST SRM981 DS (TIMS) values and the normalization factor applied to the GEOMAR sample data. Sr-Nd-Pb total chemistry blanks are below 50pg and thus considered negligible.

Oxygen isotope composition ($\delta^{18}O_{SMOW}$) of volcanic glass, olivine and plagioclase phenocrysts separated from crushed rocks was analyzed by laser fluorination at the University of Oregon. Details of the analytical technique were reported elsewhere (Bindeman et al., 2004). The overall analytical uncertainty of single measurements did not exceed 0.2 ‰ (2σ) based on replicate analyses of San Carlos olivine standard. Results are reported in Table 4.

4. RESULTS

4.1 Major and trace elements

The Tolbachik samples are basalts and basaltic trachyandesites of medium- and high-K composition, some of the most alkali-rich rocks in the CKD (Fig. 2a-b, Table 1, 2). Pre-2012 rocks are subdivided here into three major groups on the basis of a scheme modified after Flerov and Bogoyavlenskaya (1983): 1) the rocks with $MgO/Al_2O_3>0.6$ (oxides in wt%) are referred to here as High-Magnesian Basalts (HMB), 2) the rocks with $MgO/Al_2O_3<0.4$ as High-Alumina Basalts (HAB), and 3) the rocks with $MgO/Al_2O_3=0.4$-0.6 as Intermediate Basalts (INTB) (Fig. 2c).

Flerov and Bogoyavlenskaya (1983) provide comprehensive petrographic and petrochemical descriptions of Tolbachik rocks. In brief, HMB and INTB have basaltic, predominantly medium-K and transitional to high-K, compositions. Typical examples of HMB come from the Alaid, Krasny and Peschanie Gorki cones and lava flows associated with them (Table 2). HMB from the "1004" cone and the Great Tolbachik Fissure eruption in 1975-1976 have somewhat elevated K_2O content (1-1.3 wt.%) compared to HMB from other vents (Fig. 2b-c). Although these rocks have medium-K composition according to the IUGS criteria (Fig. 2b), it is practical to consider them as a K-rich sub-group of HMB and thus we term all HMB with $K_2O\geq1$ wt% as K-HMB. HMB samples range from aphyric to rare olivine- and clinopyroxene-phyric (~5 vol.% phenocrysts) with minor amounts of plagioclase. K-HMB are more porphyritic and contain up to ~10% olivine phenocrysts. Orthopyroxene was found as inclusions in olivine in one sample (K01-30). INTB are closely associated with HMB and typically precede eruption of HAB, as, for example, during the 1975-1976 eruption. INTB tend to have more phenocrysts (3-15 %) than HMB. Olivine and clinopyroxene are the dominant

phenocrysts, and plagioclase is slightly more abundant in INTB than in HMB. The HAB group includes high-K basalts and basaltic trachyandesites. HAB contain the greatest amounts of phenocrysts (5-25 %), primarily plagioclase with subordinate amounts of olivine and clinopyroxene.

Volcanic rocks from the 2012-2013 eruption are high-K basaltic trachyandesites with $MgO/Al_2O_3<0.26$ and are the most evolved rocks in the Tolbachik volcanic field. The rocks contain ~5% phenocrysts of predominantly plagioclase but also olivine and pyroxene. Detailed descriptions of the petrography and compositional variations of the rocks erupted in 2012-13 are reported in Volynets et al. (2015).

With decreasing MgO (from HMB to HAB), SiO_2, TiO_2, Al_2O_3, Na_2O, K_2O, P_2O_5, Nb, Zr, Y, Rb, Ba, LREE, Pb and Ga contents increase, whereas CaO, Cr, Ni and Sc contents decrease, while FeO, V and Zn remain roughly constant (Fig. 3, Table 2). K-HMB have lower Ca and Sc but higher concentrations of most other incompatible (e.g., K, Rb, Ba, Nb, Th, K, Pb, Zr, LREEs) and compatible trace elements (Ni, Cr) than HMB with lower K_2O. Modelled trends of fractional crystallization of potentially primary magma (HMB) (shown in Fig. 3) fail to explain significant enrichment of INTB, HAB and 2012-2013 rocks in highly incompatible elements consistent with previous studies (e.g., Volynets et al., 1983; Kadik et al., 1989; Dosseto et al., 2003). A combination of equilibrium crystallization and magma mixing (HAB-HMB) provides a closer match between the modelled and observed range of major and trace element concentrations in the Tolbachik rocks.

Copper concentrations have rarely been reported for Tolbachik rocks (2 published analyses in the CKD database; Portnyagin et al., 2007a). Our new Cu data fill this gap

and demonstrate the unusual behaviour of this element in Tolbachik rocks. Concentrations of Cu (100-250 ppm) in Tolbachik volcanic rocks are the highest compared to nearly all Quaternary volcanic rocks from Kamchatka and exhibit a crude negative correlation with MgO (Fig. 4). In contrast, Cu concentrations are <100 ppm in typical Kamchatka volcanic rocks and generally correlate positively with MgO. High Cu contents similar to those in Tolbachik rocks have only been reported for plateau basalts in Kamchatka. They belong to the basement of the Klyuchevskoy Volcanic Group (this study, sample K01-65) and to the Miocene plateau at the Left Ozernaya River in the Sredinny Range (Volynets et al., 2010) (Fig. 4). There appears to be a clear link between abundant post-magmatic Cu mineralization and strong Cu enrichment of erupted magmas in the Tolbachik field. Some plateau basalts in Kamchatka also host abundant Cu mineralization. For example, Perepelov (2004) reported native copper in voids of the shield-stage mega-plagiophyric lavas of Teklentulup volcano in the Sredinny Range.

Low-MgO (3.0-4.2 wt.%) basaltic trachyandesites from the 2012-2013 Tolbachik eruption have distinct compositions and form a distinct kink on some of the MgO versus major oxide plots, e.g. versus SiO_2, for the Tolbachik rock arrays (Fig. 3). Despite the small (<1-1.5%) difference in MgO content compared to typical HABs, the 2012-13 rocks have up to 2-times higher concentrations of highly incompatible elements (e.g., Nb, Th, U, LREEs, Rb, Zr, Cu), lower Al_2O_3, CaO, Sr, and similar to lower concentrations of Cr, Ni and Sc compared to HAB (Table 3). Concentrations of Ti, V and Fe are variable and spread from higher to lower values than in HABs. The most Si-rich rocks originate from the initial phase of the 2012-2013 eruption. The rocks from the following major eruption phase are slightly less evolved (Volynets et al., 2015; Volynets et al., 2013).

Incompatible trace elements in Tolbachik rocks exhibit spiked patterns on multi-element diagrams. As is usually observed for subduction-related magmas including those from Kamchatka (e.g., (Churikova et al., 2001; Kepezhinskas et al., 1997)), the Tolbachik rocks display enrichment of large ion lithophile elements (LILEs: Rb, Ba, K), U, Pb relative to LREE, Th, Ta and Nb, and also LREE and Th enrichment over Nb and Ta (Fig.5). The patterns (except for Sr) are subparallel to each other and illustrate an overall enrichment in incompatible elements with decreasing MgO from HMB to INTB to HAB to 2012-2013 rocks. Despite the 2-3 wt.% difference in MgO content, K-HMB and INTB exhibit similar abundances of incompatible elements.

In detail, ratios of incompatible elements vary significantly in Tolbachik rocks and correlate with MgO and K_2O contents. For example, Ba/Nb, K/Nb, La/Nb, Ba/Th decrease and Rb/Ba, Nb/Zr, Cs/Rb, Cs/Ba increase with decreasing MgO and increasing K_2O contents (Fig. 6). Fractional crystallization process cannot explain the difference in trace element ratios between HMB, HAB and 2012-2013 rocks, which must represent either derivation of the magmas from different sources or magmas evolved by more complex processes than closed-system fractional crystallization. INTB can be explained by mixing between HMB or even more primitive magma and low-Mg HAB and/or 2012-2013 magmas.

Moderately to strongly hydrothermally-altered and oxidized xenoliths and fresh basement rocks are pyroxene-plagioclase-phyric (15-40%) medium- to high-K basaltic andesites and trachyandesites with MgO ranging from ~10% to ~4% (Fig. 2, 3). The xenoliths have higher SiO_2 and lower FeO compared to Tolbachik volcanic rocks and, in this respect, are more similar to the Klyuchevskoy series rocks (Portnyagin et al., 2007a).

Megaplagiophyric high-K basaltic trachyandesite from the igneous Pleistocene basement of Tolbachik has some similarities with the 2012-2013 rocks but is less enriched in incompatible trace elements (e.g., K, P, Rb, Nb, La). Both xenoliths and basement rocks have distinctively low Rb/Ba and high Ba/Nb at a given K_2O or MgO content compared to Tolbachik rocks (Fig. 6).

4.2 Isotope ratios

The new high precision Sr-, Nd- and Pb- isotope data of Tolbachik rocks overlap previously published data (Churikova et al., 2001; Dosseto et al., 2003; Kepezhinskas et al., 1997; Kersting and Arculus, 1995; Portnyagin et al., 2007a; Turner et al., 1998). Although the data come from a larger range of rocks than the previously published data, the isotope data are less scattered, probably due to improved precision of our measurements. In particular, the Pb-DS data permit a better resolution of the unique isotopic composition of this volcanic field (Fig. 7; Table 4). The new data also allow us to resolve isotope variability among recent Tolbachik rocks and evaluate possible genetic links.

In Sr-Nd isotope coordinates, the Tolbachik compositions ($^{87}Sr/^{86}Sr$=0.703247-0.703421, $^{143}Nd/^{144}Nd$=0.513073-0.513089) fall close to the central part of a broadly triangle-shaped field of Kamchatka volcanic rocks (Fig. 7a), which occupies the right upper part of the Indian MORB array and extends towards more radiogenic Sr isotope compositions than found in MORB. Within the Kamchatka field, the Tolbachik compositions plot outside of the Indian MORB field and exhibit moderately high $^{87}Sr/^{86}Sr$, overlapping with some Sredinny Range compositions and are broadly

intermediate between the Eastern Volcanic Front (EVF) rocks (e.g. Gorely and Mutnovsky volcanoes) and more northern CKD volcanoes, Klyuchevskoy and Shiveluch. The basement and xenolith samples have the highest $^{87}Sr/^{86}Sr$ (0.70351-0.70356) of the Tolbachik rocks and show a slightly larger range in Nd-isotopic composition (0.513063-0.513089). These compositions are similar to those from Klyuchevskoy volcano, as is also the case with the major element contents.

Tolbachik rocks display very restricted ranges in Pb isotope ratios ($^{206}Pb/^{204}Pb$=18.173-18.204, $^{207}Pb/^{204}Pb$=15.470-15.476, $^{208}Pb/^{204}Pb$=38.836-38.859; n=12) and plot close to the middle part of the Kamchatka array (Fig. 7c,e), within the broad fields of the northern CKD volcanoes and Sredinny Range but are distinct from individual volcanoes from these regions. Similar to the majority of Kamchatkan rocks (except some from the Sredinny Range) with strong subduction signature, the Tolbachik rocks plot within the overlapping Indian and Pacific MORB fields on the uranogenic Pb diagram and slightly above the Northern Hemisphere Reference Line (NHRL; (Hart, 1984)) with $\Delta 7/4Pb$=0.9-1.3 (Fig. 7c). On the thorogenic Pb diagram (Fig. 7e), the rocks have $\Delta 8/4Pb$=23-25 and are displaced significantly from the Pacific MORB field and plot well above the NHRL within the Indian MORB field. Compared to more northern CKD volcanoes (Bezymianny, Klyuchevskoy, Shiveluch) and EVF volcanoes (e.g., Karymsky, Mutnovsky, Gorely), Tolbachik rocks have the least radiogenic Pb-isotope compositions. On the other hand, the Pb isotopic composition of the Tolbachik rocks is similar to the composition of xenoliths in the Bezimianny volcano andesites (Kayzar et al., 2014), which however have slightly higher $^{207}Pb/^{204}Pb$.

In detail, Tolbachik rocks exhibit some small-scale isotopic variability exceeding the analytical uncertainty (Fig. 7b,d,f). HAB from a presumably >1.7 ka lava flow has the least radiogenic Sr- and Pb-isotopic composition. Sr and Nd isotopic compositions of the other samples are very similar, although medium-K HMBs seem to have slightly less radiogenic Sr than high-K HMB, INTB and HAB. The Pb isotope ratios of the HAB, INTB and 2012-2013 rocks form good corelations, with the old HAB sample and initial 2012-2013 rocks plotting on both ends of the array. Compared to the more evolved samples, the HMB are displaced to higher $^{206}Pb/^{204}Pb$ at similar $^{207}Pb/^{204}Pb$ and $^{208}Pb/^{204}Pb$. The Pb isotope ratios thus require mixing of at least three distinct components to form the Tolbachik rocks. The ash from the initial eruptions in 2012 has slightly more radiogenic Nd and Pb-isotope composition than lavas from the main phase of the eruption in 2013. The isotopic compositions are very similar to and on average indistinguishable from that of HAB erupted in 1976.

Sr, Nd and Pb isotope ratios in Tolbachik rocks exhibit no significant correlation with MgO or other magma fractionation indices (Fig. 8a,b). The small number of samples analysed for Pb isotopes does not allow us to evaluate if the slightly higher $^{206}Pb/^{204}Pb$ in the three samples of HMB and K-HMB ($^{206}Pb/^{204}Pb$~18.20 in HMB vs. 18.17-18.19 in HAB and INTB) represent a distinct source for the HMB or simply minor isotopic variability in the primitive magmas.

Oxygen isotopic compositions were obtained for olivine separates from rocks from the pre-2012 eruptions and for plagioclase and matrix glass for the 2012-2013 eruption (Table 4). To facilitate comparison, all measured $\delta^{18}O$ were recalculated to equilibrium glass (melt). The $\delta^{18}O_{glass}$ values range from 5.8 to 6.6‰ and vary

unsystematically with MgO (Fig. 8c). The values are close to the upper limit of MORB glasses (5.4-5.8‰, (Eiler et al., 2000b)) and up to 0.8‰ higher, mostly within the range of glass in equilibrium with olivine from intra-oceanic arc basalts and andesites (Eiler et al., 2000a). The highest $\delta^{18}O_{glass}$=6.0-6.5‰ were obtained for HAB erupted in 1976 and basaltic trachyandesites from the 2012-2013 eruption. Notably, $\delta^{18}O$ of Tolbachik rocks is systematically lower and closer to MORB than it is in samples from the Klyuchevskoy volcano (Auer et al., 2009; Dorendorf et al., 2000; Portnyagin et al., 2007a).

5. DISCUSSION

5.1. Mantle and slab processes

It is generally agreed that in active subduction zones the mantle wedge partially melts due to the influx of slab fluids and/or melts released from the subducting oceanic lithosphere (Gill, 1981; Kelley et al., 2010; Portnyagin et al., 2007b; Stolper and Newman, 1994). The exact conditions at which subduction-related magmas are formed in the mantle (pressure, temperature, source composition, degrees of melting), the nature and provenance of the slab components (sources and conditions of origin, composition, physical state and its amount in the source of the magmas), and the agreement of estimated parameters with numeric models (P-T and dehydration paths of subducting slab, mantle wedge thermal state) still need to be resolved. Here we make an attempt to quantify some of these parameters for Tolbachik volcanic field using modelling software PRIMACALC2.0 and ABS3.0 (Kimura and Ariskin, 2014; Kimura et al., 2009), which integrate several modern petrological models relevant to arc magma genesis. At first we quantify the composition of primary Tolbachik magmas, estimate P-T conditions of

mantle melting, the amount of water in the source, and then quantify the relative contribution from pressure-release and fluid-fluxed melting. Then, we estimate the trace element composition of the slab component and possible conditions at which the component can be formed in the slab subducting under Kamchatka.

5.1.1. Primary magmas

The first step toward quantitative estimation of mantle melting conditions is determination of primary magma composition. Due to the occurrence of aphyric, high-magnesian rocks (MgO>10%), which represent melt composition more confidently than porphyritic or more evolved rock types, Tolbachik is one of a few arc volcanoes where the calculation of primary magma composition requires minimal extrapolation. Primary arc magmas are expected to be equilibrated with olivine Fo_{88-94} (e.g., Herzberg et al., 2007). In previous works, the primary/parental Tolbachik magmas have been assumed to have 10% MgO (Hochstaedter et al., 1996) or to be in equilibrium with olivine Fo_{91} (Portnyagin et al., 2007a). Churikova et al. (2001) estimated the degrees of mantle melting from the systematics of Ca and Na normalized to 6% MgO. To estimate a possible composition of primary Tolbachik magmas in this study, we used PRIMACALC2 program (Kimura and Ariskin, 2014), which integrated COMAGMAT-3.72 (Ariskin and Barmina, 2004) and PRIMELT2 (Herzberg and Asimow, 2008) subroutines in one package and used Fe/Mg and NiO in olivine to test equilibration of primary basalt magma with the mantle peridotite. A modified Ol-An-Qz projection from Di and FeO-MgO basalt-peridotite equilibrium from PRIMELT2 is then used to estimate degree of mantle melting (F) and pressure (P) using the primary basalt composition.

Mantle melting temperature in the hydrous system is computed by adjusting T with a parametrization for water-bearing systems (Katz et al., 2003).

A prerequisite for the correct use of the PRIMELT2 model is the origin of primary melt from mantle peridotite as opposed to olivine-free ("pyroxenite") sources, which also appear to play a role in arc magmatism (Portnyagin et al., 2009; Straub et al., 2011; Straub et al., 2008; Yogodzinski et al., 2015). Two possible criteria were proposed to distinguish the magmas originating from peridotite vs. pyroxenite source: 1) on the basis of CaO - MgO systematics, where peridotite-derived melts have CaO > 13.81-0.247*MgO (Herzberg and Asimow, 2008), and 2) on the basis of trace and major elements in high-magnesian olivine, where olivines crystallized from peridotite-derived magmas have NiO < 0.4 % and FeO/MnO<70 (Herzberg, 2010; Sobolev et al., 2007). The compositions of medium-K Tolbachik HMBs have on average ~11 wt.% CaO at ~10 wt.% MgO and plot within the field of peridotite-derived melts (Fig. 3). The CaO of K-HMB is too low to be derived from mantle peridotite (Fig. 3) and they more likely originate by mixing of HAB and magmas more primitive than HMB (see section 5.2.2). Olivine phenocrysts from both HMB and K-HMB have NiO ≤ 0.4 wt.% at Fo≤92 mol% and FeO/MnO ~ 60 (Portnyagin et al., 2009), which are consistent with the derivation of Tolbachik primary magmas from peridotite. In contrast, more northern CKD volcanoes contain olivine with Ni>0.4 wt.% and FeO/MnO>60, which indicates involvement of pyroxenite sources (Portnyagin et al., 2009).

As a starting composition for calculation of primary melt, we used the average composition of medium-K HMB analyzed in this study (Tables 2 and 5). The composition is slightly different from that calculated by averaging of all published

analyses of HMB (Portnyagin et al., 2007a), which is biased towards the composition of HMB erupted in 1975 and has slightly higher K_2O, P_2O_5 and TiO_2 compared to other Tolbachik HMB. Crystallization of primary magma was simulated at oxygen fugacity QFM+1. PRIMACALC2 predicted olivine to be the only liquidus phase up to 10 kbar pressure. The amount of H_2O in primary melt was assumed to be 2.8 wt% based on maximum H_2O content in melt inclusions from high-Fo Tolbachik olivine (Portnyagin et al., 2007b). Additional calculations were performed at 4 and 6 wt.% H_2O to evaluate the effect of H_2O on the primary melt composition.

The calculated major element composition of the primary melt (Table 5; Fig. 3) is nearly independent of the assumed H_2O content and has picritic composition (MgO=14%, SiO_2=49.7%; Table 5). Average Tolbachik HMB can be products of ~12% fractional olivine crystallization from the primary melt at any crustal depth (<35 km). The melt is predicted to have Mg#=0.72 in equilibrium with mantle olivine Fo_{91} at pressure of ~1.8 GPa (~60 km depth). At 2.8 wt.% H_2O in Tolbachik primary melts, the estimated mantle temperature is 1319^o C (Table 5), which is just 10^o C higher than the solidus temperature of dry fertile peridotite at 1.8 GPa (1308^o C, (Katz et al., 2003)). This implies that the mantle melting must be driven by the flux of H_2O-bearing, presumably, slab component (Portnyagin et al., 2007b). The amount of pressure-release melting can be estimated for Tolbachik to be less than 2%. Although significant contribution from pressure-release melting has been proposed for the CKD volcanoes due to a possible rifting and mantle upwelling (Dorendorf et al., 2000), our petrologic analysis does not support this hypothesis. The estimated mantle temperature is too low for extensive super-solidus pressure-release melting.

If some amount of H_2O was lost from the melt inclusions during slow magma ascent to shallow depths, during magma cooling after eruption and during experimental homogenization (Danyushevsky et al., 2002; Gaetani et al., 2012; Portnyagin et al., 2008a), then the initial H_2O was higher than 2.8 wt% and the estimated mantle temperature - lower than at the dry peridotite solidus (e.g., 1290 ^{o}C at 4 wt% H_2O, Table 5). Notably, the calculated NiO in liquidus olivine of Tolbachik magmas is somewhat higher at 4 wt% than at 2.8 wt% H_2O (0.37 vs. 0.29 wt.% NiO, Table 5) due to the temperature effect on the Ni partitioning between olivine and melt (Li and Ripley, 2010). The higher NiO content agrees better with the real composition of high-Fo Tolbachik olivines (Portnyagin et al., 2009) and with the origin of primary magma from a peridotite source (Herzberg, 2010; Sobolev et al., 2007; Takahashi, 1991). H_2O content in Tolbachik primary melts can thus indeed be as high as 4 wt.%. At H_2O = 6 wt.% in primary melt, NiO in olivine is predicted to be ~0.53 wt%, which is higher than in Tolbachik olivine (Portnyagin et al., 2009) (Table 5).

In comparison with more northern CKD volcanoes (Klyuchevskoy, Shiveluch, Shisheisky Complex), the Tolbachik primary melts have similar MgO but lower SiO_2, Na_2O, Mg# and higher CaO, FeO and TiO_2 (Table 5). This difference may be attributed to the involvement of pyroxenite sources in the origin of magmas north from Tolbachik (Portnyagin et al., 2007b; Portnyagin et al., 2009). Unrealistically low pressure for Shiveluch volcano and Shisheisky complex (0.8-1 GPa), corresponding to crustal depths under CKD (<35 km; (Levin et al., 2002)) and high degree of melting estimated in PRIMACALC2 can also indicate the presence of pyroxenite in the source (Kimura and Ariskin, 2014). In contrast, the primary magmas of Tolbachik and likely Ushkovsky

(Portnyagin et al., 2007b) volcanoes originate from peridotite, making these volcanoes different from their neighbours.

5.1.2. Mantle and slab components

Quantitative modelling of the isotope and trace element composition of Tolbachik primary magma requires determination of geochemically contrasting mantle and slab (sediments, igneous crust) components potentially involved in the primary magma origin. The compositions were estimated as described below and shown in Table 6 and Fig. 9, 10.

Tolbachik HMB have Nb/Y ratios in the range of 0.05-0.08 (Table 2), which are similar to those in average (DMM) to slightly enriched (E-DMM) MORB mantle (Nb=0.05-0.07 (Salters and Stracke, 2004; Workman and Hart, 2005)). Based on these data, we assumed that Tolbachik mantle source has DMM composition (Salters and Stracke, 2004) (Fig. 9).

Sr-Nd-Pb isotope composition of the mantle wedge is relatively well constrained for the northern Kamchatka (Portnyagin et al., 2005) but can be variable further south along the arc. In this work, we adopted the isotope composition of the northern Kamchatka mantle wedge (NKMW) estimated by Portnyagin et al. (2005) (Table 6, Fig. 7). Sr and Nd isotope ratios in NKMW ($^{87}Sr/^{86}Sr$~0.70281, $^{143}Nd/^{144}Nd$~0.51310) were assumed to be represented by the composition of Late Pleistocene basalt from Hailulia volcano (sample G4465), which has the smallest subduction-related signature in northern Kamchatka (Portnyagin et al., 2005). Pb isotope composition of the NKMW ($^{206}Pb/^{204}Pb$~17.8, $^{206}Pb/^{204}Pb$~15.4, $^{206}Pb/^{204}Pb$~37.7) was estimated by the extrapolation

of linear regressions of Ce/Pb vs. Pb isotope ratio correlations for the North Kamchatka rocks to the mantle Ce/Pb=25 (Portnyagin et al., 2005). Some rocks from the Sredinny Range and Nachikinsky volcano in the northermost CKD exhibit EM1-like compositions with low $^{143}Nd/^{144}Nd$ and high $^{87}Sr/^{86}Sr$ compositions (Churikova et al., 2001; Portnyagin et al., 2007a; Volynets et al., 2010) (Fig. 7). The involvement of EM1-like sources cannot be excluded for CKD magmas but appears to be minor because of their generally radiogenic Nd-isotope composition.

The Pacific Plate offshore Central Kamchatka contains the northernmost part of the Emperor Ridge (Meiji Seamount) built on Cretaceous oceanic crust, which is covered with pelagic sediments. The thickness of sediments drilled at the Meiji Seamount (DSDP site 192) is about 1000 meters, twice as large compared to the seafloor sediments subducting beneath southern Kamchatka (The shipboard scientific party, 1973). The sediments are diatomaceous silty clay and diatom ooze with volcanic ash layers (0-110 mbsf, Holocene-Pliocene), diatom ooze (110-550 mbsf, Pliocene-upper Miocene), diatom-rich clay (550-705 mbsf, lower upper to upper middle Miocene), claystone (705-940 mbsf, lower middle Miocene – Oligocene), chalk and calcareous claystone (940-1050 mbsf, upper Eocene to Cretaceous). In this work, we used the average weighted composition of the sediments (Bailey, 1996). The Nd isotopic composition of the sediments was not analysed, and therefore estimated to be $^{143}Nd/^{144}Nd \approx 0.51255$ at $^{87}Sr/^{86}Sr = 0.7065$ from the correlation of $^{87}Sr/^{86}Sr$ and $^{143}Nd/^{144}Nd$ of sediments dredged in the Kamchatka-Aleutian junction area (Bindeman et al., 2004). Pb isotopic composition of the sediments was averaged from the data on sediments from the ODP Sites 881-884 (Kersting and Arculus, 1995) and DSDP Site 193 (Bailey, 1993), which

have similar stratigraphy to DSDP Site 192. The average sediment composition is referred hereafter to as NWPS (Northwestern Pacific Sediments, Table 6). NWPS have less radiogenic Sr and Pb isotopic composition, are less enriched in REE, HFSE and Th, and have similar or higher U and LILE (K, Rb, Ba) contents compared to the Global Subducted Sediments (GLOSS; (Plank and Langmuir, 1998). The NWPS composition estimated in this work (Table 6, Fig. 9) is significantly different from that previously assumed for Kamchatka (Plank and Langmuir, 1998).

There is some evidence that older Emperor Seamounts were subducted beneath Central Kamchatka (Portnyagin et al., 2008b). Therefore, we performed our calculations with two different compositions of altered oceanic crust (AOC), using a relatively depleted MORB (MORB-AOC) and an enriched Meiji basalt (Meiji-AOC). As a possible compositional analogue of the Cretaceous MORB offshore Kamchatka, we used an average composition of altered Cretaceous (?) MORB-type basalts from the coastal Kamchatka ophiolites (Duggen et al., 2007). This composition is quite similar to that of Cretaceous MORB from ODP Site 304 offshore the southern Kuril Islands (Bailey, 1993). The Kamchatka MORB-AOC has a similar Nd and less radiogenic Pb and Sr isotopic composition compared to more conventional estimates of the Pacific AOC (Hauff et al., 2003; Kelley et al., 2003) (Fig. 7, Table 6). An average composition of Meiji basalts from DSDP Site 192 was calculated from literature data (Bindeman et al., 2004; Keller et al., 2000; Regelous et al., 2003). The Meiji basalts are moderately enriched in incompatible elements, have relatively radiogenic Pb and Sr isotope compositions within the range of altered Pacific MORB-type AOC but have distinctively lower $^{143}Nd/^{144}Nd$ (Fig. 7, Table 6). Both MORB-AOC and Meiji-AOC have distinctively

low Pb/Ce, Th/La and Rb/Ba compared to NWPS and display characteristic compositional features of seawater altered basalts, such as selective enrichment in LILE and U relative to LREE (Fig. 9).

In Sr-Nd-Pb isotope diagrams (Fig. 7), Tolbachik as well as the majority of recent Kamchatka rocks plot within the mixing triangle with NKMW, NWPS, and MORB-AOC (±Meiji-AOC) as end-members. The isotope systematics can thus be explained by mixing of these 3 (or 4) components in the magma source. The mantle wedge composition under the southern Kamchatka is, however, not well constrained. Judging from the relatively radiogenic Pb isotopic composition of Mutnovsky and Gorely volcanic rocks (Duggen et al., 2007), the Southern Kamchatka wedge may have higher $^{206}Pb/^{204}Pb$ and similar $\Delta 7/4Pb$, $\Delta 8/4Pb$, $^{87}Sr/^{86}Sr$ and $^{143}Nd/^{144}Nd$ compared to NKMW (Fig. 7). Some Quaternary rocks from the Sredinny Range plot outside the mixing triangle and require involvement of an EM1-like ("OIB") mantle component with high $\Delta 7/4Pb$, $\Delta 8/4Pb$, and low $^{143}Nd/^{144}Nd$ (Churikova et al., 2001; Volynets et al., 2010).

5.1.3. Quantitative modelling of slab dehydration and mantle melting

The modelling of the slab component composition and flux melting was performed with the ABS3 program (version 3.10ED; Kimura et al., 2010; Kimura et al., 2009). With the help of the program, we simulated fluid release and partial melting of the oceanic crust composed of NWPS, MORB-AOC and Meiji-AOC (Table 6) in the depth interval from 2 to 5 GPa and calculated trace element compositions of partial mantle melts formed at various pressures and temperatures in response to addition of up to 10% of the calculated H_2O-bearing slab liquid to the mantle wedge. Pressure-temperature (P-

T) path of the slab top beneath Kamchatka was estimated from a finite-element high-resolution model (van Keken et al., 2002).

P-T path of the subducting plate and compositions of slab-derived liquids (fluids or melts) calculated in ABS3 are shown in Fig. 10. A sharp temperature increase from 400 to 700^{o} C and massive H_2O release from the slab occurs at 2.3-2.6 GPa (76-86 km) beneath Kamchatka, where amphibole and lawsonite in AOC break down (van Keken et al., 2011)(Fig. 10a). In this pressure range, fluids released from the slab are rich in H_2O, LILE and moderately to very depleted in Th, U, LREE and thus have very high Ba/Th, K/La and Pb/Ce (Fig. 10b-g). At 2.6 GPa and ~ 700^{o}C, the slab top approaches the water-saturated solidus of AOC and terrigeneous sediments. Slab melting has dramatic effects on the composition of slab-derived liquids that at these conditions will be water-rich melts strongly enriched in LREE, Th and U, resulting in relatively low Ba/Th, Pb/Ce and K/La (Fig. 10b-g).

Ratios of highly incompatible elements (e.g., Pb/Ce, Ba/Th and K/La) in Tolbachik primary melts are very different from those in low temperature slab fluids but fall in the range of hydrous slab melts at P>2.6 GPa and T>710^{o}C. Characteristic ratios of highly incompatible trace elements in Tolbachik magmas are intermediate between those in partial NWPS and AOC-(MORB and/or Meiji) melts (Fig. 10b-g). Contribution from at least two slab lithologies (sediments and AOC) is thus required to explain trace element pattern of primary Tolbachik magmas in agreement with the Sr-Nd-Pb isotope systematics (Fig. 7).

This result is fully consistent with the growing evidence that hydrous melts (or supercritical fluids) from the subducted slab play a major role in magma genesis in

Kamchatka (Duggen et al., 2007; Plechova et al., 2011; Portnyagin et al., 2007a; Portnyagin et al., 2007b; Simon et al., 2014), which is nevertheless considered to be a "cold subduction zone" in the global systematics (Syracuse et al., 2010).

Forward ABS3 modelling of primary Tolbachik melt composition confirms these semi-quantitative observations (Fig. 11, Table 6). ABS3 found the best-fit between Tolbachik primary melt and model primary magma at a very narrow range of P-T conditions for slab and mantle melting. According to this modelling, the slab component is a mixture of partial melts from NWPS, Meiji-AOC and MORB-AOC in the proportion 5.0 : 27.5 : 67.5 wt.%, respectively, which originated at ~2.8 GPa and 725^{o} C (Fig. 11d). The amount of the slab component in the mantle source is estimated to be ~7 wt.%. The slab component introduced 0.26 wt% H_2O to the mantle peridotite and resulted in ~6% mantle peridotite melting at 2 GPa and 1250^{o} C. The primary magma is predicted to have 4 wt% H_2O in agreement with PRIMACAL2 modeling.

MORB and Meiji-AOC have similar trace element ratios (Fig. 9), and their Pb isotopic compositions plot nearly on one line with the inferred composition of the mantle wedge (Fig. 7). Therefore, relative contribution of MORB-AOC and Meiji-AOC to the Tolbachik magma source is difficult to determine quantitatively. In general, ABS3 trace element modelling with Meiji-AOC component returns a better fit for the primary Tolbachik basalt, because Meiji-AOC slab melt is more enriched in incompatible trace elements (compare Fig. 11b and Fig. 11d). High $^{143}Nd/^{144}Nd$ in Tolbachik magmas, however, cannot be explained with the low $^{143}Nd/^{144}Nd$ Meiji-AOC component and unequivocally require involvement of high $^{143}Nd/^{144}Nd$ MORB-AOC (Fig. 7). The presence of 70% MORB-AOC and 30% Meiji-AOC in the slab component yields a

reasonably good agreement for trace elements and Sr-Nd isotope ratios between the inferred Tolbachik primary melt and that calculated in ABS3 (Table 6, Fig. 11).

The oxygen isotope composition of Tolbachik magmas ($\delta^{18}O$ ~ 6 ‰) is also consistent with the model and can be explained by mixing of 7% slab component with $\delta^{18}O$ ~12 ‰ and the mantle peridotite with $\delta^{18}O$=5.6 ‰. The inferred O-isotope composition of the slab component is well within the possible range of mixtures between Meiji- and/or MORB-AOC ($\delta^{18}O$ ~ 10‰) and NWPS ($\delta^{18}O$=10-24‰) (Bindeman et al., 2004).

Calculated Pb isotopic composition of the slab liquid and primary magma are also shown in Table 6 and Fig. 7. Though the measured and calculated isotopic compositions do not match precisely (Table 6), Tolbachik rock compositions plot very close to the mixing line connecting the Pb isotope composition of the slab component, which was estimated based on fitting of trace element abundances, and NKMW. Excellent agreement between the calculated and measured rock compositions, therefore, can be achieved by adding a smaller proportion of the slab component to the mantle source, using a lower Pb concentration in the slab component and/or by adding some unradiogenic Pb from the subducting mantle peridotite to the source. It is thus possible that more complex processes, not only mixing of liquids from different slab sources as implied in ABS3, were involved in the origin of the slab component. Such processes can include, for example, reaction of liquids from the slab interior with the overlaying slab layers as the liquids migrate upwards.

5.2. Magmatic fractionation

After segregation from the mantle, subduction-related magmas undergo fractionation under polybaric crustal conditions, which can involve crustal assimilation, magma mixing and degassing (e.g., Stern, 2002). In this chapter we address some key geochemical features of Tolbachik rocks, which place important constraints on the origin of this magma series and may have implications for the interpretation of other long-lived volcanic systems.

5.2.1. No strong evidence for crustal assimilation

Assimilation is an expected process of magma interaction with crustal wall rocks and cannot be excluded for any magma series. Petrogenetic importance of crustal assimilation compared to other magma differentiation processes varies between different tectonic and volcanic settings. Crustal assimilation is an energy consuming process and should be accompanied by magma crystallization (Reiners et al., 1995; Spera and Bohrson, 2001). Therefore, the best indication of assimilation of compositionally contrasting crustal material by Tolbachik magmas would be a correlation of isotope ratios with parameters indicating crystallization.

Tolbachik rocks have a very narrow range in isotopic compositions (Fig. 7), which do not significantly correlate with MgO or other fractionation indices and differ from the composition of xenoliths in lavas (Fig. 7,8). Therefore, assimilation of a large amount of isotopically contrasting material (e.g. continental-type crust) can be excluded for Tolbachik magmas. Small-scale isotopic variations of Tolbachik rocks can originate from subtle source heterogeneity and minor crustal assimilation. These processes are, however, difficult to reconcile with the presently available data. For example, three-

component mixing, which is required to explain the observed spread of isotopic compositions of Tolbachik lavas, can be readily explained by small variations in the relative proportions of the mantle, sediment and AOC components involved during mantle and slab melting. Small contribution from crustal material with low $^{206}Pb/^{204}Pb$ and high $\Delta 7/4$, such as in crustal xenoliths from Bezimianny volcano (Kayzar et al., 2014), however, cannot be completely excluded. The large observed variations of incompatible trace element ratios in Tolbachik rocks (Fig. 6) do not correlate with the isotope ratios and therefore must have a different origin than crustal assimilation or melting of a compositionally heterogeneous mantle source.

5.2.2. Origin of Tolbachik magmas in an open magmatic system

Since the extensive petrologic studies of 1975-1976 Tolbachik eruption, it is known that Tolbachik HAB cannot be related to HMBs by simple fractional crystallization (Volynets et al., 1983; Dosetto et al., 2003; Churikova et al., 2001; Kadik et al., 1989). Most researchers consider Tolbachik HAB to have come from a different parental magma than the HMB (e.g., Churikova et al., 2001; Dosseto et al., 2003). Our modelling confirms that HAB cannot originate from medium-K HMB by single-stage fractional crystallization. The products of fractional crystallization from HMB at different fixed pressures (1 to 10 kbar) or at polybaric conditions (magma crystallizes as it rises to the surface) have FeO that is too high, SiO_2 and concentrations of incompatible elements (e.g., K, P, Ti) that are two low compared to HAB (Fig. 3). Fractional crystallization also fails to explain the large fractionation between highly incompatible trace elements in Tolbachik rocks (Fig. 6). Mysteriously, magmas erupted in 2012-2013 represent one

more, previously unknown type of Tolbachik magma, which cannot be related to either HMB or HAB by fractional crystallization (Fig. 6).

Nevertheless, since the rock types have overlapping Sr and Nd and very similar Pb isotope ratios and since they are spatially and temporally associated in the Tolbachik volcanic field, a genetic link between these three major groups of Tolbachik magmas is likely to exist. We envision two possible solutions for the paradox: (1) HAB and 2012-2013 magmas originate by fractional crystallization from K_2O-rich HMB parental magmas; (2) HAB and 2012-2013 magmas originate from medium-K HMB by open system fractional crystallization processes.

K-HMB samples that could serve as potential parents for HAB were indeed found in the Tolbachik volcanic field, e.g. Cone "1004" in our collection. Low-pressure fractional crystallization of the high-K parental magma can in principle explain the enrichment of HAB in K_2O and other highly incompatible elements. However, the existence of primary high-K melts is questionable. CaO content in K-HMB is too low for peridotite-derived parental melts (Fig. 3) inferred from olivine analysis (see section 5.1.1). Unlike the expected compositions of primary magmas (Fig. 11), K-HMB demonstrate no Sr enrichment relative to REE and exhibit trace element patterns which are essentially similar to those of INTB lavas, except that the K-HMB lavas have significantly higher Pb concentrations. These features of the K-HMB are inconsistent with those expected for a primary magma. It is more likely that K-HMB have a hybrid origin and like INTB originate by mixing of HAB and primitive medium-K magmas (e.g. Volynets et al., 1983). Because K-HMB lavas have similar MgO contents as the medium-K HMB lavas (~10 wt.%), they cannot originate by mixing of the medium-K

HMB and high-K HAB (Fig. 3, 6). A more appropriate model for the origin of K-HMB and also some INTB lavas is a mixing of HAB with more primitive magmas than HMB. For example, high-K HMB from the Cone "1004" can originate by mixing of ~40% HAB and ~60% of near primary Tolbachik magma with MgO~14 wt.% (Fig. 3, 6). Thus, K-HMB lavas are likely products of HAB and medium-K primitive magma mixing, and therefore they cannot be parental for HAB lavas.

What is then the specific crystallization process which is able to link HMB, HAB and 2012-2013 magmas? Tolbachik is a long-lived volcanic system with numerous eruptions during the past 10 ka, which predominantly had evolved compositions but periodically also HMB and hybrid compositions. Taking these observations into consideration, the model of closed-system, single-stage fractionation crystallization appears to be a gross oversimplification of the real system and therefore fails to explain the compositional variability observed. An open magmatic system (magma chamber) with periodic replenishment, magma mixing, eruption and fractional crystallization is a more realistic scenario for the Tolbachik volcanic field and is worth testing in detail. Open-system fractionation was already proposed to explain the compositions of the 1975-1976 Tolbachik eruption (Kadik et al., 1989). The open-system fractionation process has been referred to as RTF (recharge-tapping-fractionation; O'Hara, 1977; O'Hara and Mathews, 1981) or REFC (recharge-evacuation-fractional crystallization) (Lee et al., 2014). In this study we adopt the latter abbreviation to comply with the most recent literature.

Geochemical effects of REFC, which are different from those of simple closed-system fractional crystallization, have been extensively studied theoretically (Caroff et

al., 1997; Lee et al., 2014; O'Hara and Mathews, 1981; Rannou et al., 2006). Well-documented examples of the REFC-type magmatic systems are however rare. In the recent years, REFC has been invoked to explain the major and trace element variability of mid-oceanic ridge basalts (Caroff and Fleutelot, 2003; O'Neill and Jenner, 2012; Rannou et al., 2006) and rarely of arc (Chiaradia et al., 2011) and intraplate (Óladóttir et al., 2008; Yu et al., 2015) magmatic series.

Some major effects of REFC, which are important to evaluate the origin of Tolbachik magma series, are the following (Lee et al., 2014; O'Hara and Mathews, 1981): (1) existence of steady-state liquid (SSL) compositions, (2) similarity of SSL to the products of equilibrium crystallization, (3) dependence of the number of REFC cycles required to achieve SSL on the partition coefficient of element, and (4) potentially large fractionation between incompatible trace elements.

Unlike single-stage fractional crystallization with an undefined end point of crystallization, the REFC model predicts that the magma can approach a SSL composition during several REFC cycles (Fig. 13). The SSL composition is independent of the relative (but fixed) volume of mafic magma replenishments, which only influences the number of cycles necessary to achieve steady state. The majority of Tolbachik magmas are HAB with a narrow compositional range (Flerov and Bogayavlenskaya, 1983; Braitseva et al., 1983). Dominance of erupted magma with a similar composition suggests that the Tolbachik magma system (shallow magma chamber?) was close to steady state during the Holocene, which is expected for REFC-type systems.

An interesting feature of REFC systems, which is still not sufficiently appreciated by most petrologists, is that SSL compositions must lie on the same trend formed by

closed-system equilibrium crystallization of a parental magma, even though REFC represents a combination of fractional crystallization, recharge, mixing and eruption (Langmuir, 1989). Therefore, by modelling the equilibrium and fractional crystallization of the parental melt, for example, using COMAGMAT3.72 (Ariskin and Barmina, 2004), we can test between the REFC and fractional crystallization models. We present the results of the modelling in Fig. 3. The results of a simplified modelling adopting constant bulk partition coefficients for major and trace elements (Lee et al., 2014) are shown in Fig. 13. The latter approach allowed us to find intermediate REFC compositions and to evaluate the number of REFC cycles required to achieve SSL compositions. The simplified modelling was performed for MgO and a number of trace elements. Bulk solid-liquid partition coefficient for MgO (D_{Mg}) was set to 2.8, which provides a close approximation for the variable D_{Mg} in the range of compositions between 4 and 10 wt.% MgO (Fig. 12a). Partition coefficients for trace elements were compiled from literature sources (Table 3). Calculation of REFC has been performed using Excel spread sheets from Lee et al. (2014).

The trend of equilibrium crystallization (=SSL) closely approaches typical HAB compositions and predicts well the high concentrations of incompatible elements (TiO_2, K_2O, P_2O_5) and also low FeO at relatively high MgO in HAB (Fig. 3, 13). Therefore typical Tolbachik HAB can be interpreted as approaching the SSL compositions of REFC magmatic system fed by medium-K primary magma. The range of element concentrations at a given MgO in Tolbachik rocks (Fig. 3, 4, 13) is also consistent with the REFC model and reflects a different number of cycles to approach SSL for compatible ($D_i>1$) and incompatible ($D_i<1$) elements. For example, SSL corresponding to

an average Tolbachik HAB with MgO~5 wt.% is achieved at a ratio of crystallized over erupted magma of ~0.7 after 3 REFC cycles. Up to 20 cycles are required for K_2O to achieve SSL with K_2O~2 wt.% at the same conditions. Periodic eruption of hybrid (INTB, K-HMB) and primitive (HMB) magmas provides further support for recharging and mixing occurring in the system, which are necessary components of REFC.

Strong enrichment of Tolbachik magmas in copper implies that it remains incompatible during magma fractionation (Fig. 4). A major host for copper in magmatic systems are sulphide phases (Li and Audetat, 2012; Liu et al., 2015). An incompatible behaviour of Cu implies that sulphide phases were not stable during Tolbachik magma evolution. Primitive Tolbachik melts have high sulphur content (>2500 ppm) (Portnyagin et al., 2007b). The absence of sulphide on the liquidus of such sulphur-rich magmas most likely reflects unusually oxidizing conditions (Jugo, 2009; Lee et al., 2012). In absence of magnetite, Fe^{3+} behaves as an incompatible element during magma fractionation, and therefore REFC system can evolve to more oxidizing conditions than predicted by fractional crystallization (Lee et al., 2014). The unusual Cu enrichment in Tolbachik magmas may thus be a consequence of magma oxidation (Lee et al., 2012) resulting from open system conditions (REFC). Similar compositions of Tolbachik magmas and plateau basalts in Kamchatka, including Cu enrichment, suggest that REFC processes could have played a major role during periods of voluminous volcanism in Kamchatka related to formation of large basaltic plateaus in the Late Miocene – Early Quaternary time.

Compared to fractional crystallization, REFC predicts significant fractionation of incompatible elements at moderate depletion in MgO (Fig. 13). This fractionation is strongly controlled by the partitioning of elements between crystallizing phases and melt

(D_i). Therefore, a strong correlation is expected between the variability of trace elements in a magmatic series and their partition coefficients, though the exact trend is dependent on the exact type of the crystallization process (Schiano et al., 1993). In contrast, the variability produced by mixing of different sources (assimilation, mixing of distinct mantle melts) is not expected to correlate with the crystal-liquid partition coefficients. Appropriate partition coefficients for trace elements in Tolbachik magmas (Table 3) are plotted against their variability in Tolbachik magmas in Fig. 12b. Variability of trace elements is defined as the ratio of one standard deviation over the mean value (Schiano et al., 1993) and is calculated using high precision ICP-MS data (Table 6). A strong correlation between variability and D_i supports crystallization processes controlling the variability of trace element ratios in the Tolbachik magmas.

D_i's listed in Table 3 have been used to test the viability of different processes to explain the trace element variability in the Tolbachik rocks. As an example, modelling of Ba/Nb in Tolbachik magmas is presented in Fig. 13b. REFC predicts a convex trend of significantly decreasing Ba/Nb with decreasing MgO and an increase in the ratio of crystallized over erupted magma. It can explain the whole range of Ba/Nb observed in Tolbachik rocks. In contrast, HAB and HMB mixing forms a concave trend. Mixing of HAB and HMB can most easily generate INTB and K-HMB compositions, whereas REFC processes can most closely generate HAB and 2012-2013 rock compositions.

Although the REFC model predicts very well the major compositional features of the Tolbachik rock series, we note some inconsistency between the estimated model REFC parameters using absolute concentrations of incompatible elements and their ratios (Fig. 13). Our model results, however, are strongly dependent on the partition

coefficients, which are not precisely known for Tolbachik magmas and mostly taken from a study of MORB (O'Neill and Jenner, 2012). In order to improve the modelling results, the partition coefficients should be determined precisely and specifically for Tolbachik magmas, for example, using melt inclusions in minerals (Sobolev et al., 1996).

Complimentary to REFC, additional fractionation between incompatible trace elements can result from in-situ fractionation within the magma chamber (Langmuir, 1989). In-situ fractionation involves crystallization on the walls of the magma chamber coupled with continuous extraction of evolved melt from the crystallized margins and mixing of this melt with the melts in the magma chamber interior. Large fractionation between incompatible elements by the in-situ fractionation, significantly exceeding that by REFC, requires effective extraction of melts from strongly crystallized cumulates (>70% crystals). Extraction of melts from magma crystallized by more than 30%, especially at low-pressure and water-saturated conditions, is hardly possible due to small density contrast between the interstitial melt and the parental melt (Kuritani, 2009). Nevertheless, in-situ fractionation may contribute to the variability of Tolbachik magmas and can perhaps partly explain some discrepancies in the REFC modelling.

5.2.3. Origin of the 2012-2013 volcanic rocks: a decrease in recharge to the Tolbachik magma system?

The magmas erupted in 2012-2013 have distinctively more evolved compositions compared to typical Tolbachik HABs (Fig. 3). These rocks have Sr-Nd-Pb isotope compositions very similar to HAB erupted in 1976 and thus could be interpreted as magmas evolved by fractional crystallization from 1976 HAB during the following 36

years. This intuitively appealing model, however, fails to explain the difference in ratios of highly incompatible elements between HAB and 2012-2013 rocks (Fig. 6, 13). In accordance with the REFC model, which we favour for the long-term evolution of the Tolbachik magmatic system, the shift to more evolved compositions during the 2012-2013 eruption implies that the steady state composition of the magma reservoir has probably changed since 1976. The reason for the change may be delayed eruption or less abundant mafic replenishment of the Tolbachik magma chamber after the 1975-1976 eruption. Notably, the compositions of 1976 HAB (MgO~4.5 wt%) are more evolved compared to average Holocene HAB of the Tolbachik field (MgO~5 wt%) (Flerov and Bogoyavlenskaya, 1983). Therefore, the 2012-2013 andesites (MgO~4 wt%) follow the historic trend towards even more evolved compositions. This trend may reflect a decreasing rate of mafic recharge to the Tolbachik magma system during the Holocene.

6. CONCLUSIONS

Primary middle-K, mantle-derived picrite magmas with ~14 wt% MgO and up to ~4% H_2O have fed the long-lasting volcanism in the Tolbachik volcanic system. The primary magmas originate through partial melting of mantle peridotite in the mantle wedge at ~1250^o C and 1.8-2.0 GPa, reflecting pressure and temperature conditions below the dry peridotite solidus. The low temperature mantle melting under Tolbachik is triggered by slab-derived hydrous slab melt originating at ~2.8 GPa and ~720^{o}C. Sr-Nd-Pb isotope and trace element systematics suggest contribution from three to four components (reservoirs) to the primary Tolbachik magmas: 1) Indian-type depleted

mantle, 2) subducted Northwest Pacific sediments, 3) MORB-type and/or 4) Meiji-type altered oceanic crust.

Fractionation of primary magmas within the crust generated the range of Tolbachik volcanic rocks, which comprise medium-K high-Mg basalts, high-K high-Mg basalts, basaltic trachyandesites and intermediate rock varieties. Single-stage fractional crystallization ± crustal assimilation ± source variability fail to explain the narrow range of Sr-Nd-Pb-O isotopic composition and large range between highly incompatible elements in Tolbachik volcanic rocks. A fundamental process capable of explaining all major compositional features of the Tolbachik rocks is open system fractionation, which occurred with periodic recharge of evolved magma with primitive magma from depth, mixing, fractional crystallization and periodic eruption (Recharge-Evacuation-Fractional Crystallization; REFC system). High-K, low-Mg basalts, which predominate in the Tolbachik volcanic field, approach steady-state REFC compositions. Mixing of the evolved high-Al basalts and more mafic (10-14 wt.% MgO) magmas, periodically replenishing the evolved Tolbachik magma chamber, can generate the array of intermediate rock compositions, including K-rich high-Mg basalts.

High-K basaltic trachyandesites, unusual for the Tolbachik volcanic field, were erupted in 2012-2013. These magmas cannot be related to the more common high-K basalts by fractional crystallization. These evolved magmas are interpreted to be products of REFC, formed under conditions of diminished primary magma supply from depth and/or delayed eruption since the Great Fissure Tolbachik eruption of 1975-1976.

REFC processes result in strong enrichment of evolved magmas in incompatible trace elements and likely also in oxidation of the magmas. Magma oxidation can explain

unusual enrichment of Tolbachik rocks in Cu and possibly other chalcophile elements (Au, Ag, As, etc.) and the close association of the Tolbachik volcanism with post-magmatic Cu mineralization. Similar Cu enrichment and likely mineralization are anticipated for plateau basalts in Kamchatka.

An important result of Tolbachik magma fractionation by the REFC scenario is the strong fractionation between incompatible trace elements (e.g., Rb/Ba, La/Nb, Ba/Th), which is often assigned to source variability or crustal assimilation. Some geochemical features of arc volcanoes should be critically evaluated in light of the new data and do not necessarily require geochemical variability of the parental magmas. The studies aimed at evaluation of magma source composition and melting processes should be restricted to the analysis of the most primitive high-magnesian rocks and/or melt inclusions in high-magnesian (Fo>88) olivine.

This study shows that subduction-related, long-lived volcanic systems, such as the Tolbachik volcanic field, reflect multi-component dynamic mantle melting and open-system evolution in crustal reservoirs. Open-system models provide more plausible and precise description of such magmatic systems than simpler but often geologically unrealistic closed-system, single-stage scenarios.

ACKNOWLEDGEMENTS

Our sincere thanks go to our colleagues from the Institute of Volcanology and Seismology (Kamchatka, Russia) for long-term collaboration and support: D. Melnikov, D. Savelyev and N. Gorbach for generous donation of samples from the 2012-2013 Tolbachik eruption, to S. Khubunaya for his expert guidance during our first field season

in Tolbachik volcanic field in 2001, to V. Ponomareva and A. Volynets for helpful discussion of various aspects of the paper. We are grateful to D. Rau, D. Garbe-Schönberg, U. Westernströer and S. Hauff for their assistance with XRF, ICP-MS and isotope analysis, to L. Heuer for sample preparation, and to C. Roberts for his help with the clean lab procedures at RHUL. E. Zelenin (Geologic Institute, Moscow) is thanked for digital map processing. Jun-Ichi Kimura and an anonymous reviewer provided detailed and helpful comments on the early version of this manuscript. The field work was supported by the Russian Foundation for Basic Research. S.D. was funded by the UK Royal Society/Leverhulme Trust Senior Research Fellowship to M.F.T. and by the German Science Foundation to S.D. (DU426/1-1,2; DU426/3-1) and K.H. (HO1833/16-1). The Russian Science Foundation provided support to M.P. and N.M. (grant no. 14-17-000582).

REFERENCES

Ariskin, A.A. and Barmina, G.S., 2004. COMAGMAT: Development of a Magma Crystallization Model and Its Petrological Applications. Geochem. Inter., Vol. 42, Suppl. 1: S1–S157.

Ariskin, A.A., Barmina, G.S., Ozerov, A.Y. and Nielsen, R.L., 1995. Genesis of high-alumina basalts from Klyuchevskoi volcano. Petrology, 3: 496-521.

Auer, S.L., Bindeman, I., Wallace, P., Ponomareva, V.V. and Portnyagin, M., 2009. The Origin of Hydrous, high-δ18O voluminous volcanism: Diverse Oxygen Isotope Values and High Magmatic Water Contents within the Volcanic Record of

Klyuchevskoy Volcano, Kamchatka, Russia. Contrib. Mineral. Petrol., 157(2): 209-230, doi:210.1007/s00410-00008-00330-00410.

Bailey, J.C., 1993. Geochemical History of Sediments in the Northwestern Pacific-Ocean. Geochem. J., 27(2): 71-90.

Bailey, J.C., 1996. Role of subducted sediments in the genesis of Kurile-Kamchatka island arc basalts: Sr isotopic and elemental evidence. Geochem. J., 30(5): 289-321.

Baker, J., Peate, D., Waight, T. and Meyzen, C., 2004. Pb isotopic analysis of standards and samples using a Pb-207-Pb-204 double spike and thallium to correct for mass bias with a double-focusing MC-ICP-MS. Chem. Geol., 211(3-4): 275-303.

Baker, J.A., Peate, D.W., Waight, T.E. and Thirlwall, M.F., 2005. Reply to the: Comment on "Pb isotopic analysis of standards and samples using a Pb-207-Pb-204 double spike and thallium to correct for mass bias with a double focusing MC-ICP-MS" by Baker et al. Chem. Geol., 217(1-2): 175-179.

Balesta, S.T., 1981. Crust and magmatic chambers in the areas of modern volcanism. Nauka, Moscow, 132 pp.

Belousov, A., Belousova, M., Edwards, B., Volynets, A. and Melnikov, D., 2015. Overview of the precursors and dynamics of the 2012-13 basaltic fissure eruption of Tolbachik Volcano, Kamchatka, Russia. J. Volcanol. Geotherm. Res., 299: 19-34, doi:10.1016/j.jvolgeores.2015.1004.1009.

Bindeman, I.N., Ponomareva, V.V., Bailey, J.C. and Valley, J.W., 2004. Volcanic arc of Kamchatka: a province with high- d18 O magma sources and large-scale

18O/16O depletion of the upper crust. Geochim. Cosmochim. Acta, 68(4): 841-865.

Braitseva, O.A., Melekestsev, I.V. and Ponomareva, V.V., 1983. Age divisions of the Holocene volcanic formations of the Tolbachik Valley. In: S.P. Fedotov, Ye.K. Marchinin (Editors), The Great Tolbachik Fissure Eruption: geological and geophysical data 1975-1976. Cambridge Earth Science Series, Cambridge, pp. 83-95.

Caroff, M. and Fleutelot, C., 2003. The north-south propagating spreading center of the North Fiji Basin. Modeling of the geochemical evolution in periodically replenished and tapped magma chambers. Mineral. Petrol., 79(3-4): 203-224.

Caroff, M., Lagabrielle, Y., Spadea, P. and Auzende, J.M., 1997. Geochemical modeling of nonsteady-state magma chambers: A case study from an ultrafast spreading ridge, East Pacific Rise, 17-19 degrees S. Geochim. Cosmochim. Acta, 61(20): 4367-4374.

Chiaradia, M., Muntener, O. and Beate, B., 2011. Enriched Basaltic Andesites from Mid-crustal Fractional Crystallization, Recharge, and Assimilation (Pilavo Volcano, Western Cordillera of Ecuador). J. Petrol., 52(6): 1107-1141.

Churikova, T., Dorendorf, F. and Worner, G., 2001. Sources and fluids in the mantle wedge below Kamchatka, evidence from across-arc geochemical variation. J. Petrol., 42(8): 1567-1593.

Churikova, T.G., Gordeychik, B.N., Edwards, B., Ponomareva, V.V. and Zelenin, E., this volume. The Tolbachik volcanic massif: a review of the petrology, volcanology and eruption history prior to the 2012-2013 eruption. J. Volcanol. Geotherm. Res.

Class, C. and Lehnert, K., 2012. PetDB Expert MORB (Mid-Ocean Ridge Basalt) Compilation. EarthChem Library: http://dx.doi.org/10.1594/IEDA/100060.

Danyushevsky, L., McNeill, A.W. and Sobolev, A.V., 2002. Experimental and petrological studies of melt inclusions in phenocrysts from mantle-derived magmas: an overview of techniques, advantages and complications. Chem. Geol., 183: 5-24.

Dorendorf, F., Wiechert, U. and Worner, G., 2000. Hydrated sub-arc mantle: a source for the Kluchevskoy volcano, Kamchatka/Russia. Earth Planet. Sci. Lett., 175: 69-86.

Dosseto, A., Bourdon, B., Joron, J.-L. and Dupre, B., 2003. U-Th-Pa-Ra study of the Kamchatka arc: New constraints on the genesis of arc lavas. Geochim. Cosmochim. Acta, 67(15): 2857-2877, doi:2810.1016/S0016-7037(2803)00086-00083.

Duggen, S., Portnyagin, M., Baker, J., Ulfbeck, D., Hoernle, K., Garbe-Schönberg, D. and Grassineau, N., 2007. Drastic shift in lava geochemistry in the volcanic-front to rear-arc region of the Southern Kamchatkan subduction zone: Evidence for the transition from slab surface dehydration to sediment melting. Geochim. Cosmochim. Acta, 71: 452-480.

Edwards, B., Belousov, A., Belousova, M., Volynets, A., Melnikov, D., Chirkov, S., Senyukov, S., Gordeev, E., Muraviev, Y., Izbekov, P. and Demianchuk, Y., 2013. Another “Great Tolbachik” Eruption? Eos, Transactions American Geophysical Union, 94(21): 189-191.

Eiler, J., 2001. Oxigen Isotope variations of basaltic lavas and upper mantle rocks. In: J.W. Valley and D.R. Cole (Editors), Stable isotope geochemistry. Reviews in

Mineralogy and geochemistry. Mineralogical Society of America, Geochemical Society, pp. 319-364.

Eiler, J.M., Crawford, A., Elliott, T., Farley, K.A., Valley, J.W. and Stolper, E.M., 2000a. Oxygen Isotope Geochemistry of Oceanic-Arc Lavas. J. Petrol., 41(2): 239-256.

Eiler, J.M., Schiano, P., Kitchen, N. and Stolper, E.M., 2000b. Oxygen-isotope evidence for recycled crust in the sources of mid-ocean-ridge basalts. Nature, 403: 530-534.

Fedotov, S.P. and Markhinin, Y.K. (Eds.), 1983. The Great Tolbachik Fissure Eruption: geological and geophysical data 1975-1976. Cambridge Earth Science Series, Cambridge, 341 p.

Flerov G.B., Bogayavlenskaya G.Ye., 1983, Geology and petrochemistry of the Tolbachik regional zone of cinder cones. In: S.P. Fedotov, Ye.K. Marchinin (Editors), The Great Tolbachik Fissure Eruption: geological and geophysical data 1975-1976. Cambridge Earth Science Series, Cambridge, pp. 96-115.

Gaetani, G.A., O'Leary, J.A., Shimizu, N., Bucholz, C.E. and Newville, M., 2012. Rapid reequilibration of H2O and oxygen fugacity in olivine-hosted melt inclusions. Geology, 40(10): 915-918.

Galer, S.J.G., 1999. Optimal double and triple spiking for high precision lead isotopic measurement. Chem. Geol., 157(3-4): 255-274.

Garbe-Schönberg, D., 1993. Simultaneous determination of 37 trace elements in 28 international rock standards by ICP-MS. Geostandards Newsletter, 17: 81-93.

GEOROC, 2014. Geochemistry of Rocks of the oceans and Continents, http://georoc.mpch-mainz.gwdg.de/georoc/Start.asp.

Gill, J.B., 1981. Orogenic andesites and plate tectonics. Springer-Verlag, Berlin-Heidelberg, 390 pp.

Gorbatov, A., Kostoglodov, V., Suarez, G. and Gordeev, E., 1997. Seismicity and structure of the Kamchatka subduction zone. J. Geophys. Res., 102(B8): 17833-17898.

Hart, S.R., 1984. A large-scale isotope anomaly in the Southern Hemisphere mantle. Nature, 309: 753-757.

Hauff, F., Hoernle, K. and Schmidt, A., 2003. Sr-Nd-Pb composition of Mesozoic Pacific oceanic crust (Site 1149 and 801, ODP Leg 185): Implications for alteration of ocean crust and the input into the Izu-Bonin-Mariana subduction system. Geochem. Geophys. Geosyst., 4(8), 8913: doi:10.1029/2002GC000421.

Herzberg, C., 2010. Identification of Source Lithology in the Hawaiian and Canary Islands: Implications for Origins. J. Petrology, 52(1): 113-146.

Herzberg, C. and Asimow, P.D., 2008. Petrology of some oceanic island basalts: PRIMELT2.XLS software for primary magma calculation. Geochemistry Geophysics Geosystems, 9.

Herzberg, C., Asimow, P.D., Arndt, N., Niu, Y., Lesher, C.M., Fitton, J.G., Cheadle, M.J. and Saunders, A.D., 2007. Temperatures in ambient mantle and plumes: Constraints from basalts, picrites, and komatiites. Geochem. Geophys. Geosyst., 8, Q02006, doi:10.1029/2006GC001390.

Hochstaedter, A.G., Kepezhinskas, P., Defant, M., Drummond, M. and Koloskov, A., 1996. Insights into the volcanic arc mantle wedge from magnesian lavas from the

Kamchatka arc. Journal of Geophysical Research - Solid Earth, 101(B1): 697-712.

Hoernle, K., Abt, D.L., Fischer, K.M., Nichols, H., Hauff, F., Abers, G.A., van den Bogaard, P., Heydolph, K., Alvarado, G., Protti, M. and Strauch, W., 2008. Arc-parallel flow in the mantle wedge beneath Costa Rica and Nicaragua. Nature, 451(7182): 1094-1097, doi:1010.1038/nature06550.

Hoernle, K., Hauff, F., Kokfelt, T.F., Haase, K., Garbe-Schönberg, D. and Werner, R., 2011. On- and off-axis chemical heterogeneities along the South Atlantic Mid-Ocean-Ridge (5–11°S): Shallow or deep recycling of ocean crust and/or intraplate volcanism? Earth Planet. Sci. Lett., 306(1–2): 86-97.

Hofmann, A.W., 1997. Mantle geochemistry: the message from oceanic volcanism. Nature, 385: 219-229.

Jugo, P.J., 2009. Sulfur content at sulfide saturation in oxidized magmas. Geology, 37: 415-418, doi:410.1130/G25527A.25521.

Kadik, A.A., Lukanin, O.A. and Lapin, I.B., 1989. Physical-chemical conditions of differentiation of basaltic magmas in near-surface chambers. Nauka, Moscow, 346 (in Russian) pp.

Katz, R.F., Spiegelman, M. and Lagmuir, C.H., 2003. A new parameterization of hydrous mantle melting. Geochem. Geophys. Geosyst., 4(9): 1073, doi:1010.1029/2002GC000433.

Kayzar, T.M., Nelson, B.K., Bachmann, O., Bauer, A.M. and Izbekov, P.E., 2014. Deciphering petrogenic processes using Pb isotope ratios from time-series

samples at Bezymianny and Klyuchevskoy volcanoes, Central Kamchatka Depression. Contrib. Mineral. Petrol., 168(4).

Keller, R.A., Fisk, M.R. and White, W.M., 2000. Isotopic evidence for Late Cretaceous plume-ridge interaction at the Hawaiian hotspot. Nature, 405(8 JUNE 2000): 673-676.

Kelley, K.A., Plank, T., Ludden, J. and Staudigel, H., 2003. Composition of altered oceanic crust at ODP Sites 801 and 1149. Geochemistry, Geophysics, Geosystems, 4(6): 8910.

Kelley, K.A., Plank, T., Newman, S., Stolper, E.M., Grove, T.L., Parman, S. and Hauri, E.H., 2010. Mantle Melting as a Function of Water Content beneath the Mariana Arc. J. Petrol., 51(8): 1711-1738.

Kepezhinskas, P., McDermott, F., Defant, M.J., Hochstaedter, A., Drummond, M.S., Hawkesworth, C.J., Koloskov, A., Maury, R.C. and Bellon, H., 1997. Trace element and Sr-Nd-Pb isotopic constraints on a three-component model of Kamchatka Arc petrogenesis. Geochim. Cosmochim. Acta, 61(3): 577-600.

Kersting, A.B., 1995. Pb isotope ratios of North Pacific sedimennts, sites 881, 883, and 884: Implications for sediment recycling in the Kamchatkan Arc. In: D.K. Rea, I.A. Basov, D.W. Scholl and J.F. Allan (Editors), Proceedings of the Ocean Drilling Program, Scientific Results, pp. 383-388.

Kersting, A.B. and Arculus, R.J., 1994. Klyuchevskoy volcano, Kamchatka, Russia: the role of high-flux recharged, tapped, and fractionated magma chamber(s) in the genesis of high-Al_2O_3 from high-MgO basalt. J. Petrol., 35: 1-41.

Kersting, A.B. and Arculus, R.J., 1995. Pb isotope composition of Klyuchevskoy volcano, Kamchatka and North Pacific sediments: Implications fr magma genesis and crustal recycling in the Kamchatkan arc. Earth Planet. Sci. Lett., 136: 133-148.

Kimura, J.-I., Kent, A.J.R., Rowe, M.C., Katakuse, M., Nakano, F., Hacker, B.R., van Keken, P.E., Kawabata, H. and Stern, R.J., 2010. Origin of cross-chain geochemical variation in Quaternary lavas from the northern Izu arc: Using a quantitative mass balance approach to identify mantle sources and mantle wedge processes. Geochem. Geophys. Geosyst., 11(10): Q10011.

Kimura, J.I. and Ariskin, A.A., 2014. Calculation of water-bearing primary basalt and estimation of source mantle conditions beneath arcs: PRIMACALC2 model for WINDOWS. Geochemistry Geophysics Geosystems, 15(4): 1494-1514.

Kimura, J.I., Gill, J.B., Kunikiyo, T., Osaka, I., Shimoshioiri, Y., Katakuse, M., Kakubuchi, S., Nagao, T., Furuyama, K., Kamei, A., Kawabata, H., Nakajima, J., van Keken, P.E. and Stern, R.J., 2014. Diverse magmatic effects of subducting a hot slab in SW Japan: Results from forward modeling. Geochemistry Geophysics Geosystems, 15(3): 691-739.

Kimura, J.I., Hacker, B.R., van Keken, P.E., Kawabata, H., Yoshida, T. and Stern, R.J., 2009. Arc Basalt Simulator version 2, a simulation for slab dehydration and fluid-fluxed mantle melting for arc basalts: Modeling scheme and application. Geochemistry Geophysics Geosystems, 10.

Kuritani, T., 2009. The relative roles of boundary layer fractionation and homogeneous fractionation in cooling basaltic magma chambers. Lithos, 110(1-4): 247-261.

Langmuir, C.H., 1989. Geochemical Consequences of Insitu Crystallization. Nature, 340(6230): 199-205.

Le Maitre, R.W., Streckeisen, A., Zanetti, B., Le Bas, M.J., Bonin, B., Bateman, P., Bellieni, G., Dudek, A., Efremova, S., Keller, J., Lameyre, J., Sabine, P.A., Schmid, R., Soerensen, H. and Wooley, A.R. (Editors), 2002. Igneous rocks. A classification and glossary of terms. Cambridge University Press, 236 pp.

Lee, C.-T.A., Luffi, P., Chin, E.J., Bouchet, R., Dasgupta, R., Morton, D.M., Le Roux, V., Yin, Q.-z. and Jin, D., 2012. Copper Systematics in Arc Magmas and Implications for Crust-Mantle Differentiation. Science, 336(6077): 64-68.

Lee, C.T.A., Lee, T.C. and Wu, C.T., 2014. Modeling the compositional evolution of recharging, evacuating, and fractionating (REFC) magma chambers: Implications for differentiation of arc magmas. Geochim. Cosmochim. Acta, 143: 8-22.

Levin, V., Park, J., Brandon, M., Lees, J., Peyton, V., Gordeev, E. and Ozerov, A., 2002. Crust and upper mantle of Kamchatka from teleseismic receiver functions. Tectonophysics, 358(1-4): 233-265.

Li, C.S. and Ripley, E.M., 2010. The relative effects of composition and temperature on olivine-liquid Ni partitioning: Statistical deconvolution and implications for petrologic modeling. Chem. Geol., 275(1-2): 99-104.

Li, Y. and Audetat, A., 2012. Partitioning of V, Mn, Co, Ni, Cu, Zn, As, Mo, Ag, Sn, Sb, W, Au, Pb, and Bi between sulfide phases and hydrous basanite melt at upper mantle conditions. Earth Planet. Sci. Lett., 355: 327-340.

Liu, X., Xiong, X., Audétat, A. and Li, Y., 2015. Partitioning of Cu between mafic minerals, Fe–Ti oxides and intermediate to felsic melts. Geochim. Cosmochim. Acta, 151(0): 86-102.

Meyers, J.D. and Johnston, A.D., 1996. Phase equilibria constraints on models of subduction zone magmatism. In: G.E. Bebout, D.W. Scholl, S.H. Kirby and J.P. Platt (Editors), Subduction. Top to Bottom. American Geophysical Union, Washington D.C., pp. 229-249.

O'Hara, M.J., 1977. Geochemical evolution during fractional crystallization of a periodically refilled magma chamber. Nature, 266: 503-507.

O'Hara, M.J. and Mathews, R.E., 1981. Geochemical Evolution in an Advancing, Periodically Replenished, Periodically Tapped, Continuously Fractionated Magma Chamber. Journal of the Geological Society, 138(May): 237-277.

O'Neill, H.S. and Jenner, F.E., 2012. The global pattern of trace-element distributions in ocean floor basalts. Nature, 491(7426): 698-+.

Óladóttir, B., Sigmarsson, O., Larsen, G. and Thordarson, T., 2008. Katla volcano, Iceland: magma composition, dynamics and eruption frequency as recorded by Holocene tephra layers. Bull. Volcanol., 70(4): 475-493.

Ozerov, A.Y., 2000. The evolution of high-alumina basalts of the Klyuchevskoy volcano, Kamchatka, Russia, based on microprobe analyses of mineral inclusions. J. Volcanol. Geotherm. Res., 95: 65–79.

Plank, T. and Langmuir, C.H., 1998. The chemical composition of subducting sediment and its consequences for the crust and mantle. Chem. Geol., 143: 325-394.

Plechova, A.A., Portnyagin, M.V. and Bazanova, L.I., 2011. The Origin and Evolution of the Parental Magmas of Frontal Volcanoes in Kamchatka: Evidence from Magmatic Inclusions in Olivine from Zhupanovsky Volcano. Geochem. Inter., 49(8): 743–768, DOI: 710.1134/S0016702911080064.

Ponomareva, V., Portnyagin, M., Derkachev, A., Juschus, O., Garbe-Schönberg, D. and Nürnberg, D., 2013. Identification of a widespread Kamchatkan tephra: a mid-Pleistocene tie-point between Arctic and Pacific paleoclimatic records. Geophysical Research Letters, 40: 3538-3543, DOI: 3510.1002/grl.50645.

Ponomareva, V.V., Churikova, T.V., I., M., Braitseva, O., Pevzner, M.M. and Sulerzhitsky, L.D., 2007. Late Pleistocene-Holocene Volcanism on the Kamchatka Peninsula, Northwest Pacific Region. In: J. Eichelberger, E. Gordeev, M. Kasahara, P. Izbekov and J. Lees (Editors), Volcanism and Subduction: The Kamchatka Region. American Geophysical Union, Washington D.C., pp. 165-198.

Portnyagin, M., Hoernle, K., Avdeiko, G., Hauff, F., Werner, R., Bindeman, I., Uspensky, V. and Garbe-Schonberg, D., 2005. Transition from arc to oceanic magmatism at the Kamchatka-Aleutian junction. Geology, 33(1): 25-28.

Portnyagin, M., Bindeman, I., Hoernle, K. and Hauff, F., 2007a. Geochemistry of primitive lavas of the Central Kamchatka Depression: Magma Generation at the Edge of the Pacific Plate. In: J. Eichelberger, E. Gordeev, M. Kasahara, P. Izbekov and J. Lees (Editors), Volcanism and Subduction: The Kamchatka Region. American Geophysical Union, Washington D.C., pp. 203-244.

Portnyagin, M.V., Hoernle, K., Plechov, P.Y., Mironov, N.L. and Khubunaya, S.A., 2007b. Constraints on mantle melting and composition and nature of slab components in volcanic arcs from volatiles (H2O, S, Cl, F) and trace elements in melt inclusions from the Kamchatka Arc. Earth Planet. Sci. Lett., 255(1-2): 53-69.

Portnyagin, M., Almeev, R., Matveev, S. and Holtz, F., 2008a. Experimental evidence for rapid water exchange between melt inclusions in olivine and host magma. Earth Planet. Sci. Lett., 272: 541-552, doi:510.1016/j.epsl.2008.1005.1020.

Portnyagin, M., Savelyev, D., Hoernle, K., Hauff, F. and Garbe-Schönberg, D., 2008b. Mid-Cretaceous Hawaiian tholeiites preserved in Kamchatka. Geology, 36(11): 903-906.

Portnyagin, M.V., Sobolev, A.V., Mironov, N.L. and Hoernle, K., 2009. Pyroxenite melts involved in magma genesis in Kamchatka. 19th Annual V.M. Goldschmidt Conference, Davos, Switzerland, June 21-26, Geochimica Cosmochimica Acta, 73(13, Supp. 1): A1044, Talk.

Rannou, E., Caroff, M. and Cordier, C., 2006. A geochemical approach to model periodically replenished magma chambers: Does oscillatory supply account for the magmatic evolution of EPR 17-19 degrees S? Geochim. Cosmochim. Acta, 70(18): 4783-4796.

Regelous, M., Hofmann, A.W., Abouchami, W. and Galer, S.J.G., 2003. Geochemistry of lavas from the Emperor Seamounts, and the geochemical evolution of Hawaiian Magmatism from 85 to 42 Ma. J. Petrol., 44(1): 113-140.

Reiners, P.W., Nelson, B.K. and Ghiorso, M.S., 1995. Assimilation of Felsic Crust by Basaltic Magma - Thermal Limits and Extents of Crustal Contamination of Mantle-Derived Magmas. Geology, 23(6): 563-566.

Salters, V.J.M. and Shimizu, N., 1988. World-wide occurrence of HFSE-depleted mantle. Geochim. Cosmochim. Acta, 52: 2177-2182.

Salters, V.J.M. and Stracke, A., 2004. Composition of the depleted mantle. Geochem. Geophys. Geosyst., 5(5): Q05004, doi:05010.01029/02003GC000597.

Schiano, P., Allegre, C.J., Dupre, B., Lewin, E. and Joron, J.L., 1993. Variability of Trace-Elements in Basaltic Suites. Earth Planet. Sci. Lett., 119(1-2): 37-51.

Simon, A., Yogodzinski, G.M., Robertson, K., Smith, E., Selyangin, O., Kiryukhin, A., Mulcahy, S.R. and Walker, J.D., 2014. Evolution and genesis of volcanic rocks from Mutnovsky Volcano, Kamchatka. J. Volcanol. Geotherm. Res., 286: 116-137.

Sobolev, A.V., Hofmann, A.W., Kuzmin, D.V., Yaxley, G.M., Arndt, N.T., Chung, S.-L., Danyushevsky, L.V., Elliott, T., Frey, F.A., Garcia, M.O., Gurenko, A.A., Kamenetsky, V.S., Kerr, A.C., Krivolutskaya, N.A., Matvienkov, V.V., Nikogosian, I.K., Rocholl, A., Sigurdsson, I.A., Sushchevskaya, N.M. and Teklay, M., 2007. The Amount of Recycled Crust in Sources of Mantle-Derived Melts. Science, 316(5823): 412-417.

Sobolev, A.V., Migdisov, A.A. and Portnyagin, M.V., 1996. Incompatible Element Partitioning between Clinopyroxene and Basalt Liquid Revealed by the Study of Melt Inclusions in Minerals from Troodos Lavas, Cyprus. Petrology, 4(3): 326-336.

Spera, F.J. and Bohrson, W.A., 2001. Energy-constrained open-system magmatic processes I: General model and energy-constrained assimilation and fractional crystallisation (EC-AFC) formulation. J. Petrol., 42(5): 999-1018.

Stern, R.J., 2002. Subduction zones. Rev. Geophys., 40(4), 1012, doi:10.1029/2001RG000108.

Stolper, E. and Newman, S., 1994. The role of water in the petrogenesis of Mariana Trough magmas. Earth Planet. Sci. Lett., 121(3-4): 293-325.

Straub, S.M., Gomez-Tuena, A., Stuart, F.M., Zellmer, G.F., Espinasa-Perena, R., Cai, Y. and Iizuka, Y., 2011. Formation of hybrid arc andesites beneath thick continental crust. Earth Planet. Sci. Lett., 303(3–4): 337-347.

Straub, S.M., LaGatta, A.B., Martin-Del Pozzo, A.L. and Langmuir, C.H., 2008. Evidence from high-Ni olivines for a hybridized peridotite/pyroxenite source for orogenic andesites from the central Mexican Volcanic Belt, . Geochem. Geophys. Geosyst., 9, Q03007, doi:10.1029/2007GC001583.

Syracuse, E.M. and Abers, G.A., 2006. Global compilation of variations in slab depth beneath arc volcanoes and implications. Geochem. Geophys. Geosyst., 7(Q05017): doi:10.1029/2005GC001045.

Syracuse, E.M., van Keken, P.E. and Abers, G.A., 2010. The Global Range of Subduction Zone Thermal Models. PEPI, 183(1-2): 73-90.

Takahashi, N., 1991. Origin of three peridotite suites from Horoman peridotite complex, Hokkaido, Japan; Melting, melt segregation and solidification processes in the upper mantle. J. Min. Petr. Econ. Geol., 86: 199-215.

The shipboard scientific party, 1973. Site 192, Initial Reports DSDP 19. Washington (U.S. Govt. Printing Office), pp. 463-553.

Thirlwall, M., 1991a. High-precision multicollector isotopic analysis of low levels of Nd as oxide. Chemical Geology: Isotope Geoscience section, 94(1): 13-22.

Thirlwall, M., 1991b. Long-term reproducibility of multicollector Sr and Nd isotope ratio analysis. Chemical Geology: Isotope Geoscience section, 94(2): 85-104.

Thirlwall, M.F., 2000. Inter-laboratory and other errors in Ph isotope analyses investigated using a Pb-207-Pb-204 double spike. Chem. Geol., 163(1-4): 299-322.

Turner, S., McDermott, F., Hawkesworth, C. and Kepezhinskas, P., 1998. A U-series study of lavas from Kamchatka and the Aleutians: constraints on source composition and melting processes. Contrib. Mineral. Petrol., 133: 217-234.

van Keken, P.E., Hacker, B.R., Syracuse, E.M. and Abers, G.A., 2011. Subduction factory: 4. Depth-dependent flux of H2O from subducting slabs worldwide. J. Geophys. Res., 116(B1): B01401, doi:01410.01029/02010JB007922. .

van Keken, P.E., Kiefer, B. and Peacock, S.M., 2002. High resolution models for subduction zones: implications for mineral dehydration reactions and the transport of water into deep mantle. Geochemistry, Geophysics, Geosystems, 3(10): 1056, doi:1010.1029/2001GC000256.

Volynets, A., Churikova, T., Wörner, G., Gordeychik, B. and Layer, P., 2010. Mafic Late Miocene–Quaternary volcanic rocks in the Kamchatka back arc region: implications for subduction geometry and slab history at the Pacific–Aleutian junction. Contrib. Mineral. Petrol., 159(5): 659-687.

Volynets, A.O., Edwards, B.R., Melnikov, D., Yakushev, A. and Griboedova, I., 2015. Monitoring of the volcanic rock compositions during the 2012-2013 fissure eruption at Tolbachik volcano, Kamchatka. J. Volcanol. Geotherm. Res.: this volume.

Volynets, A.O., Melnikov, D.V. and Yakushev, A.I., 2013. First data on composition of the volcanic rocks of the IVS 50th anniversary Fissure Tolbachik eruption (Kamchatka). Doklady Earth Sciences, 452(1): 953-957.

Volynets, O.N., 1994. Geochemical types, petrology, and genesis of the late Cenozoic volcanic rocks from the Kurile-Kamchatka island-arc system. International Geology Review, 36(4): 373-403.

Volynets, O.N., Flerov, G.B., Andreev, V.N., Popolitov, E.I., Abramov, V.A., Petrov, L.L., Shcheka, S.A. and Selivanova G.I., 1983. Geochemical features of the rocks of the Great Tolbachik Fissure Eruption 1975-1976 in relation to petrogenesis. In: S.P. Fedotov, Ye.K. Marchinin (Editors), The Great Tolbachik Fissure Eruption: geological and geophysical data 1975-1976. Cambridge Earth Science Series, Cambridge, pp. 116-140.

Workman, R.K. and Hart, S.R., 2005. Major and trace element composition of the depleted MORB mantle (DMM). Earth Planet. Sci. Lett., 231(1-2): 53-72.

Yogodzinski, G.M., Brown, S.T., Kelemen, P.B., Vervoort, J.D., Portnyagin, M., Sims, K.W.W., Hoernle, K., Jicha, B.R. and Werner, R., 2015. The Role of Subducted Basalt in the Source of Island Arc Magmas: Evidence from Seafloor Lavas of the Western Aleutians. J. Petrol., 56(3): 441-492.

Yu, X., Lee, C.-T.A., Chen, L.-H. and Zeng, G., 2015. Magmatic recharge in continental flood basalts: Insights from the Chifeng igneous province in Inner Mongolia. Geochemistry, Geophysics, Geosystems: doi:10.1002/2015GC005805.

FIGURES

Figure 1. Geologic map of the Tolbachik volcanic field showing sample locations. The map was processed with GIS software and based on the original work of Braiteseva et al. (1983). The outline of the 2012-2013 lava flows and the lava subdivision into age groups was modified from Churikova et al. (this volume). Inset shows Kamchatka Peninsula, its major volcanic zones (Sredinny Range, CKD - Central Kamchatka Depression, EVF – Eastern Volcanic Front) and selected Quaternary volcanoes mentioned in text. The box shows the location of the detailed map (main figure).

Figure 2. Classification diagrams for Tolbachik rocks.

a) TAS (total silica versus alkalis) and b) SiO_2 vs. K_2O diagrams after (Le Maitre et al., 2002). Compositional fields of basalt (B), basaltic andesite (BA), trachybasalt (TB), basaltic trachyandesite (BTA) are shown.

c) Classification diagram for Tolbachik rocks based on MgO/Al_2O_3 and K_2O content. The scheme is modified after (Flerov and Bogoyavlenskaya, 1983). High-magnesian basalts with $MgO/Al_2O_3>0.6$ are subdivided into groups of K-rich high-magnesian basalts ($K_2O\geq1$ wt%, K-HMB) and normal high-magnesian basalts ($K_2O<1$ wt%, HMB). Intermediate basalts (INTB) have MgO/Al_2O_3 = 0.4-0.6. High-alumina basaltic trachyandesites (HAB) including rocks of 2012-2013 eruption (Volynets et al., 2013) have MgO/Al_2O_3 <0.4.

The composition of xenoliths in Tolbachik rocks, Pleistocene basement lavas (both from this study) and CKD rocks (Portnyagin et al., 2007a) are shown for comparison.

Figure 3. Variations of major elements in Tolbachik rocks in comparison with modelled magma crystallization and mixing trends. Modelling of crystallization was performed in COMAGMAT3.72 (Ariskin and Barmina, 2004). Starting composition was primary Tolbachik magma with 2 wt.% H_2O (Table 5). Oxygen fugacity was set to NNO+1 (externally buffered open system). FC – fractional crystallization, EC – equilibrium crystallization. Crystallization pressure was varied from 1 to 10 kbar. *Thick red line* (FC 10-1 kbar) refers to polybaric crystallization starting at 10 kbar at a rate of ~5.5 mol. % crystallization per 1 kbar pressure change. *Thick gray line* denotes mixing between HAB and primary melt.

Fractional crystallization (thin lines) fails to reproduce HAB and the 2012-2013 rock compositions at any pressure. Equilibrium crystallization (bold dash line) approaches the compositions similar to HAB and the 2012-2013 rocks after >50 mol.% crystallization. Evolved Tolbachik rocks may thus represent products of crystallization in REFC system (replenishment, eruption, fractionation crystallization) (see section 5.2.2 for discussion). K-HMB and INTB cannot be generated by fractional crystallization alone and therefore most likely represent mixtures of HAB and HMB or more primitive magmas. Solid green line in MgO vs. CaO diagram separates compositional fields of primary melts from peridotite (PRD) and pyroxenite (PXT) sources (Herzberg and Asimow, 2008).

Figure 4. MgO and Cu contents in Tolbachik volcanic rocks, compared with other volcanoes in Kamchatka. Kamchatka rock compositions are compiled from numerous

sources (GEOROC, 2014; Portnyagin et al., 2007a). The compositions of plateau basalts from the Left Ozernaya River area are from Volynets et al. (2010).

Figure 5. Multi-element diagram showing the incompatible trace element composition of Tolbachik rocks normalized to N-MORB (Hofmann, 1997). MgO content in rocks is denoted on the right side of each pattern. Note overall poor correlation between the incompatible trace elements and MgO and large variations at low MgO, unexpected from fractional crystallization process.

Figure 6. Variations of incompatible trace element ratios in Tolbachik volcanic rocks. Curved lines with circles show mixing trajectories calculated with 10% steps (1 – primary melt – HAB, 2 – HMB-HAB, 3- HMB – 2012-2013 rocks). Dashed line with arrow denoted general trend of fractional crystallization (FC). FC fails to explain the large variability of trace element ratios correlating with MgO and K_2O. REFC can explain the variations between HMB, HAB and 2012-2013 rocks. Magma mixing can explain the origin of intermediate rocks varieties (K-HMB, INTB) (see section 5.2.2. for discussion)

Figure 7. Sr-Nd-Pb isotopic composition of Tolbachik rocks.

Reference data: Pacific and Indian fresh MORB (Class and Lehnert, 2012), Pacific AOC (Hauff et al., 2003), North West Pacific Sediments (NWPS) (Bailey, 1996; Bindeman et al., 2004; Kersting, 1995), Meiji rocks (Keller et al., 2000; Regelous et al., 2003), MORB-AOC - average altered MORB from Kamchatka ophiolite (Duggen et al.,

2007), North Kamchatka Mantle Wedge (KMW) (see text and Portnyagin et al. 2005), Mutnovsky and Gorely volcanoes (Duggen et al., 2007), Karymsky, Klyuchevskoy, Bezyminny and xenoliths from Bezyminny rocks (Kayzar et al., 2014), North Central Kamchatka Depression (NCKD: Nachikinsky and Hailulia volcanoes and associated monogenetic volcanic cones; (Portnyagin et al., 2007a; Portnyagin et al., 2005), Srediny Range of Kamchatka (Churikova et al., 2001; Volynets et al., 2010). Pb-isotope data from (Kayzar et al., 2014) and NCKD (Portnyagin et al., 2005) data were normalized to long-term GEOMAR SRM NIST981 values (see chapter 3). NHRL – North Hemisphere Reference Line (Hart, 1984). Thin red lines in (a), (c) and (e) enclose possible compositions produced by mixing between KMW, NWPS, Meiji-AOC and MORB-AOC. Small isotopic variations in Tolbachik rocks can be explained by slightly variable proportion of KMW, NWPS and AOC in the mantle source.

Figure 8. MgO versus (a) $^{87}Sr/^{86}Sr$, (b) $^{206}Pb/^{204}Pb$ and (c) melt $\delta^{18}O$ in whole rock samples from the Tolbachik lava field. $\delta^{18}O$ in olivine and plagioclase were recalculated to $\delta^{18}O$ in equilibrium melt (glass) using $\Delta\delta^{18}O_{glass\text{-}olivine}=0.4$ and $\Delta\delta^{18}O_{glass\text{-}plagioclase}= -0.3$ (Eiler et al., 2000a). $\delta^{18}O$ measured in glass are plotted without correction. Reference data: mid-ocean ridge basalts (MORB 5.4-5.8‰, (Eiler, 2001)), oceanic island-arc basalts and andesites (IAB-A 5.3-6.4‰; (Eiler et al., 2000a)), Klyuchevskoy rocks (Auer et al., 2009; Dorendorf et al., 2000; Portnyagin et al., 2007a).

Figure 9. Incompatible trace elements in the potential end-member source components involved in the magma origin in Kamchatka. North Kamchatka mantle wedge (NKMW)

is assumed to have DMM composition (Salters and Shimizu, 1988). The compositions of NWPS, Meiji-type AOC and MORB-type AOC are estimated using literature data (see caption to Fig. 7 and section 5.1.2.).

Figure 10. Pressure-temperature path of the slab subducting beneath Kamchatka and variations of trace elements in slab-derived liquids.

Plot (a) shows P-T path of the slab top beneath Kamchatka (van Keken et al., 2002). Phase relationships in AOC, water-saturated solidus (*thick solid black line*) and dehydration solidus (*thick dashed black line*) are shown after (Kimura et al., 2009) and references therein). Thin coloured lines show stability limits of some rock-forming phases in AOC: chlorite (Chl), amphibole (Am), lawsonite (Law), phengite (Pheng). White star denotes possible conditions (a) and the composition (b-g) of the slab component involved in the origin of Tolbachik primary magmas. Plots (b)-(g) show trace element composition of slab-derived liquids (water-bearing fluids and melts) with increasing depth as calculated in ABS3 (Kimura et al., 2010). The slab-derived liquids are water-rich fluids at pressures less than 2.6 GPa and water-bearing melts at higher pressures. The compositions of slab liquids are calculated for pure source compositions corresponding to NWPS, Meiji-AOC and MORB-AOC. Low Ba/Th, Th/La, Pb/Ce and K/La in the Tolbachik primary melt (*white star*) indicate that the slab component involved in their origin is water-bearing melt formed at pressures ≥2.6 GPa. The composition of primary Tolbachik magma requires contribution from different slab lithologies, including subducted sediments.

Figure 11. Trace element composition of the Tolbachik primary melt, model fluids/melts from subducting slab and model mantle melt. Modelling was performed using the ABS3 program (Kimura et al., 2010). Symbols: *red small circles* - Tolbachik primary melt, *green triangles* – slab component, *large open circles* – calculated primary melt formed by 6% melting of KMW at 2 GPa and 1250^{o}C at addition of 7% slab fluid/melt. In plots (a), (b) and (c), slab liquids originate from pure endmember sources: NWPS, Meij-AOC and MORB-AOC, respectively. Modelling with composite fluid formed by mixture of 5% NWPS, 67.5% MORB-AOC and 27.5% Meiji-AOC derived melts provides the best match between the primary melt estimated from rock compositions and modeled in ABS3.

Figure 12. Constraints on major and trace element partitioning in the Tolbachik magma series. a) Comparison of the results of fractional crystallization obtained with constant D_{Mg} (D_{Mg}=2, 2.8, 4, 5) and using COMAGMAT3.72 at different crystallization pressures (1, 5 and 10 kbar). b) Variability of trace elements in Tolbachik rock series plotted versus bulk partition coefficient (Table 3). The strong correlation suggests that partition coefficients exert the primary control on the trace element variability. Best-fit regression line for the data is described by exponential function with equation shown on the plot.

Figure 13. Evidence for the origin of Tolbachik series in an open magmatic system. *Small circles* are literature data for the Tolbachik rocks (Portnyagin et al., 2007a). *Bold red line* shows trend for single-stage fractional crystallization (FC). *Bold green line* shows trend of REFC steady-state liquids (SSL). SSL correspond to the products of

equilibrium crystallization (EC) from the same parental melt. Numbered circles on the SSL trend denote different ratios of crystallized magma relative to erupted magma. The numbers also exactly correspond to degrees of equilibrium crystallization. *Thin blue lines* denote trends for intermediate products of REFC (REFC liquids). *Bold grey line* denotes mixing between HMB and HAB. See section 5.2.2. for detailed discussion for the major role of REFC and magma mixing in the origin of Tolbachik magma series.

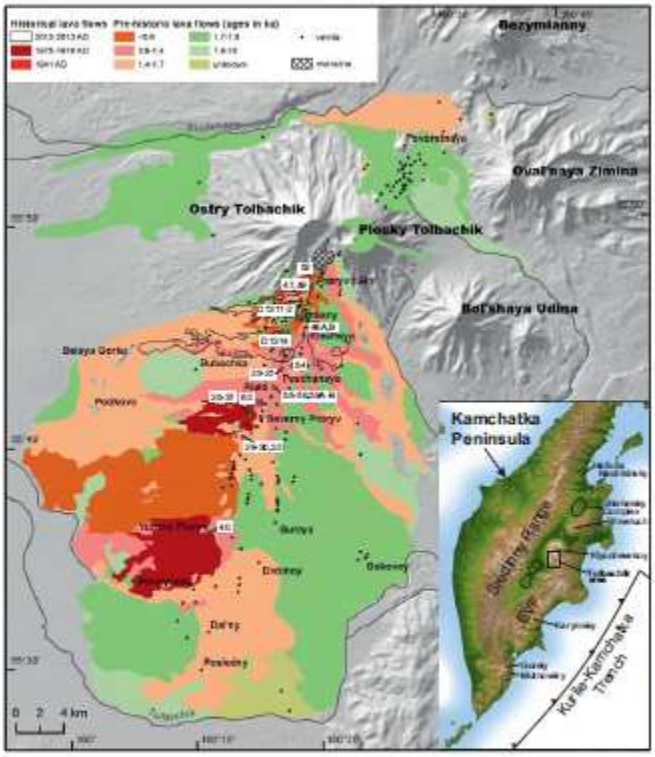

Fig. 1 (Portnyagin/Tolbachik)

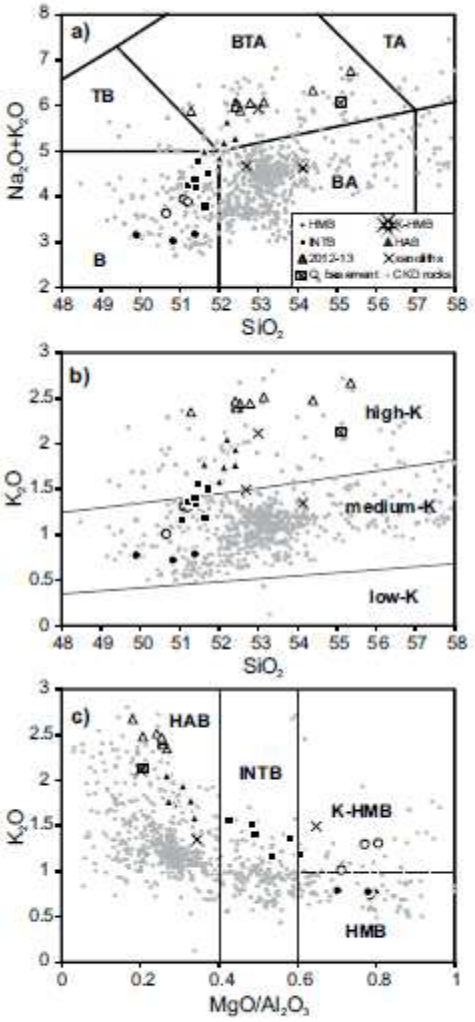

Fig. 2 (Portnyagin/Tolbachik)

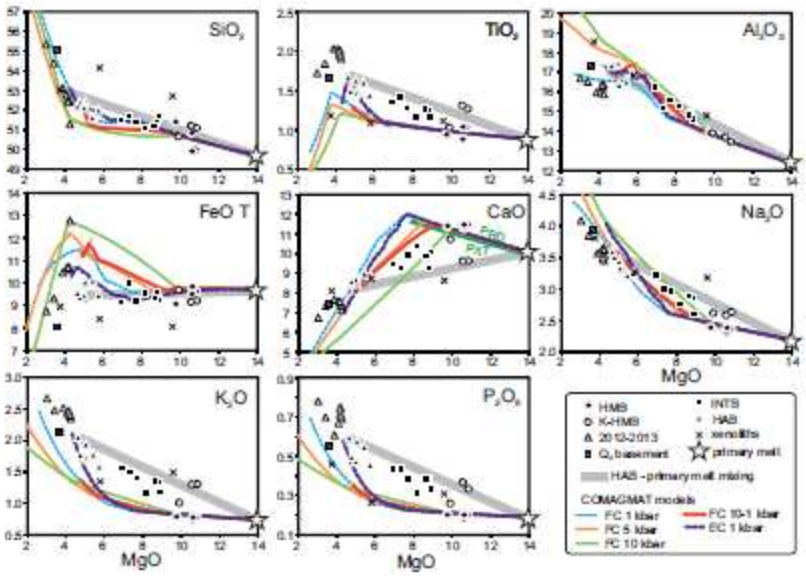

Fig. 3 (Portnyagin/Tolbachik)

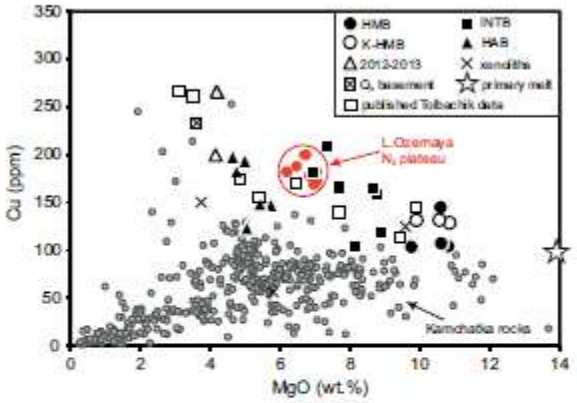

Fig. 4 (Portnyagin/Tolbachik)

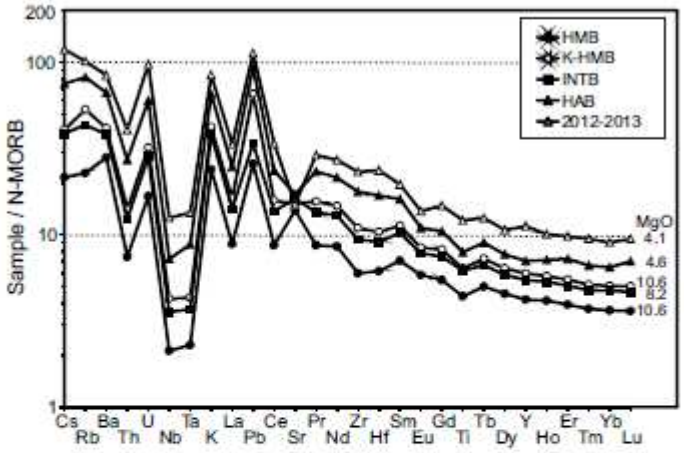

Fig. 5 (Portnyagin/Tolbachik)

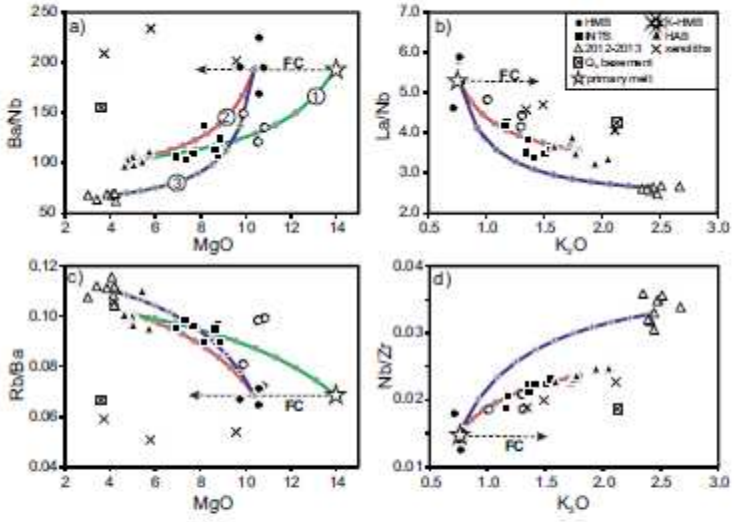

Fig. 6 (Portnyagin/Tolbachik)

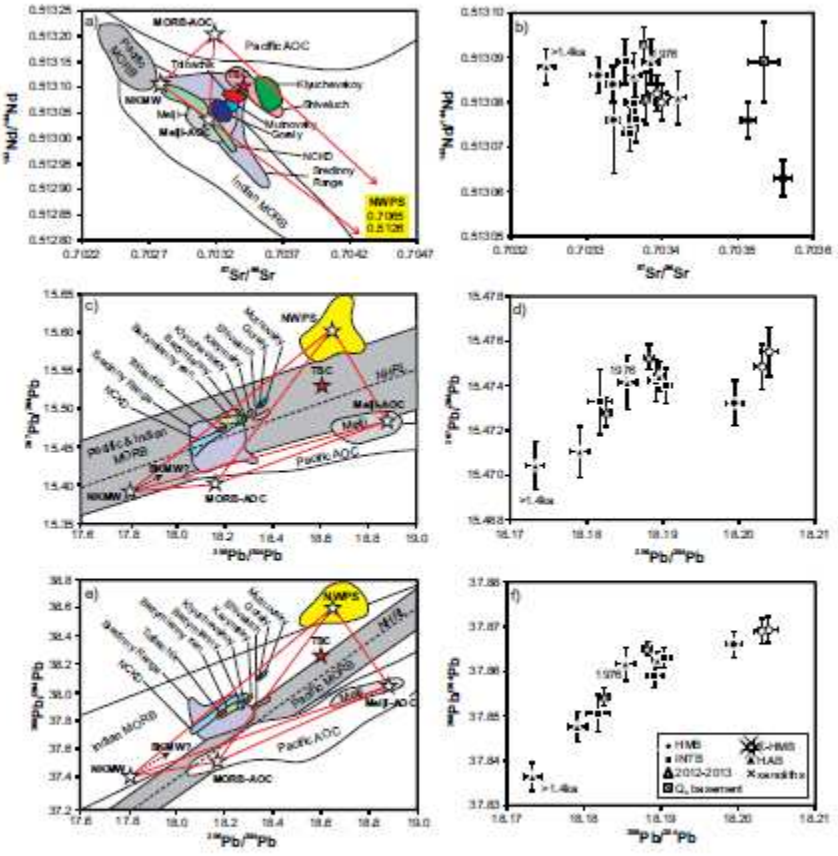

Fig. 7 (Portnyagin/Tolbachik)

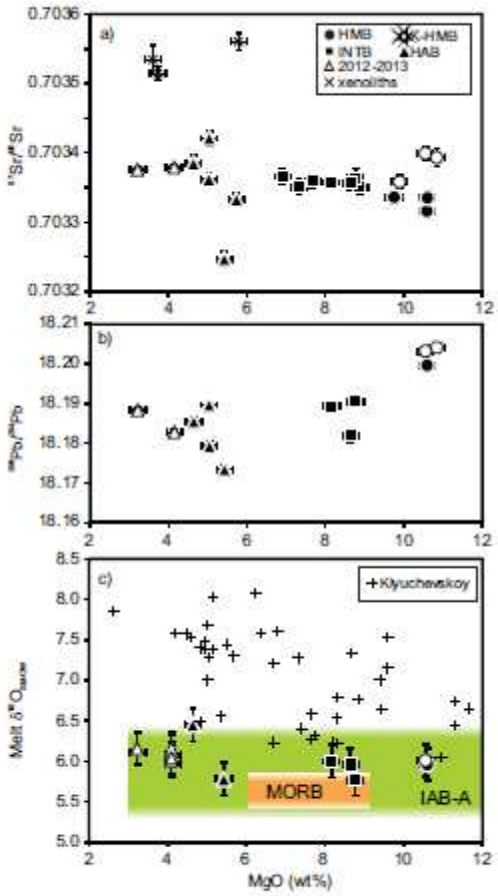

Fig. 8 (Portnyagin/Tolbachik)

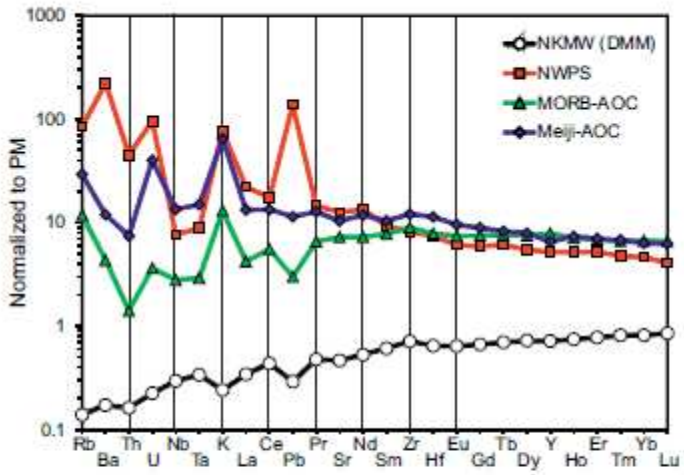

Fig.9 (Portnyagin/Tolbachik)

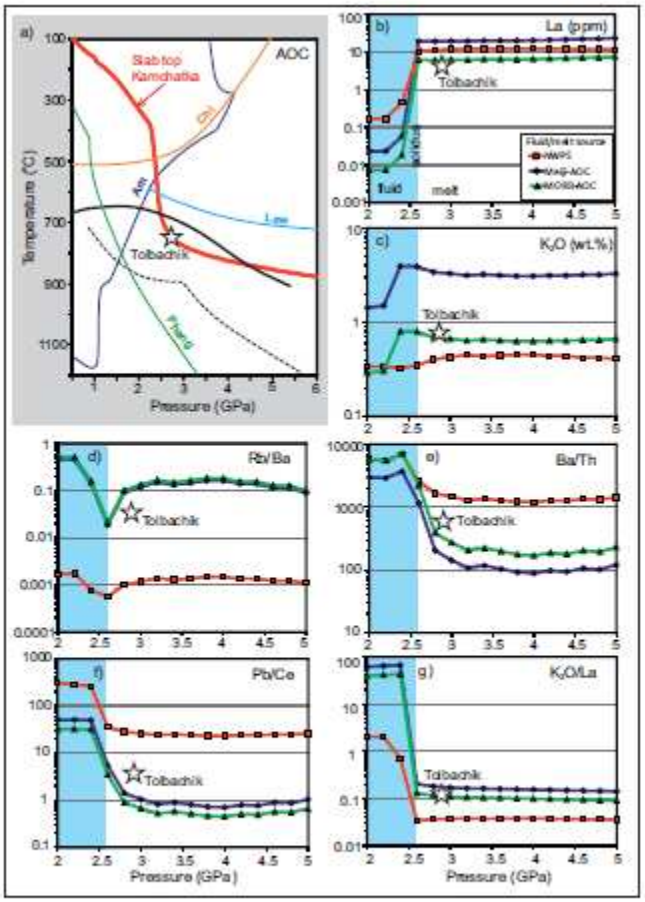

Fig. 10 (Portnyagin/Tolbachik)

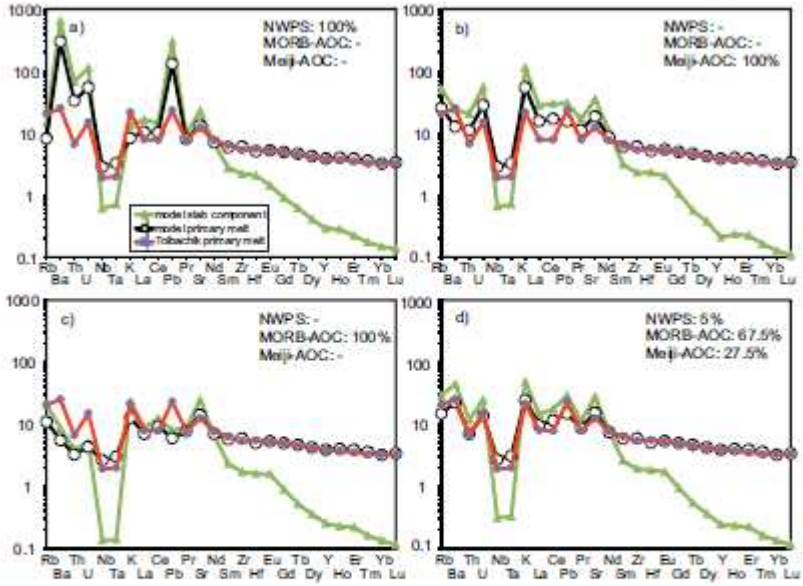

Fig. 11 (Portnyagin/Tolbachik)

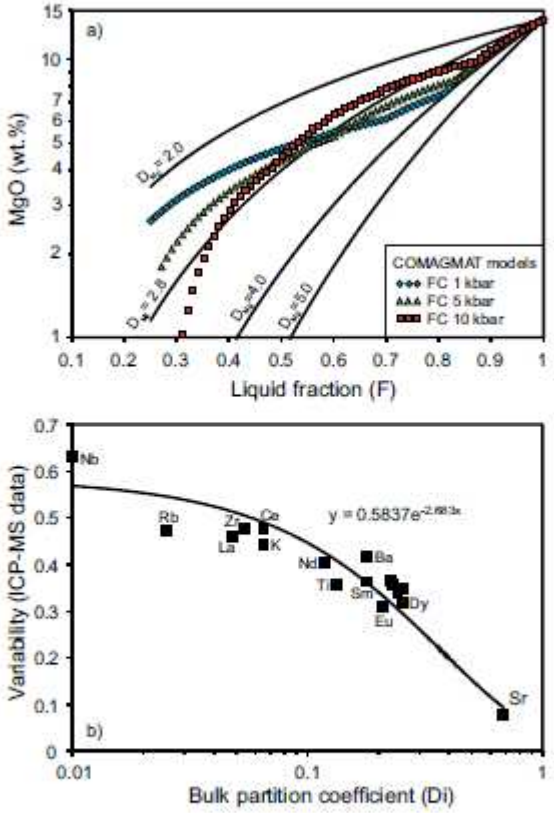

Fig. 12 (Portnyagin/Tolbachik)

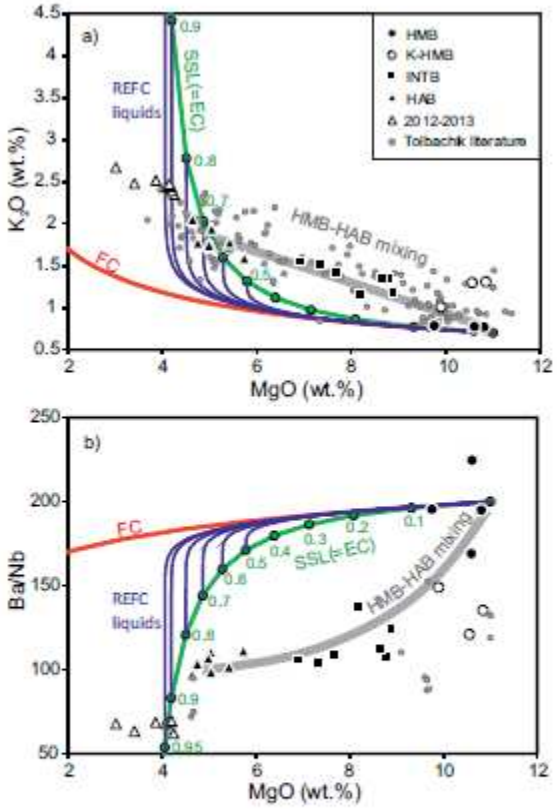

Fig. 13 (Portnyagin/Tolbachik)

Table 1. Description of rock samples from the Tolbachik volcanic field and adjacent area.

Sample	Age	Location/Cone	Lat (deg.N)	Long (deg.E)	Occurence	Rock type
K01-46B	<0.8 ka	Krasny cone	55.7611	160.3163	lava	HMB
K01-29	1.4-1.7 ka	1004 cone	55.6725	160.2401	lava	K-HMB
K01-25	0.8-1.4 ka	Peschanie Gorki cone	55.7223	160.2892	lava	HMB
K01-46A	<0.8 ka	Krasny cone	55.7611	160.3163	lava	HMB
K01-30	1.4-1.7 ka	1004 cone	55.6725	160.2401	lava	K-HMB
K01-35	1975 AD	Northern vent, cone 2	55.6857	160.2387	bomb	K-HMB
K01-56	0.8-1.4 ka	Alaid cone	55.7110	160.2734	lava	HMB
K01-57	0.8-1.4 ka	Alaid cone	55.7110	160.2734	lava	INTB
K01-58	0.8-1.4 ka	Alaid cone	55.7138	160.2753	bomb	INTB
K01-52	1941 AD	1941 cone, bomb field	55.7878	160.3353	bomb	INTB
K01-54	0.8-1.7 ka	Pelmen cone	55.7250	160.2983	lava	INTB
K01-37	1975-76	Northern vent, cone 2	55.6857	160.2387	bomb	INTB
K01-59A	1-1.5 ka	Alaid cone	55.7062	160.2745	lava	INTB
K01-34	1975 AD	Northern vent, cone 2	55.6857	160.2387	bomb	INTB
K01-59B	0.8-1.4 ka	Alaid cone	55.7062	160.2745	lava	HAB
K01-49	1.7-7.8 ka	lava field	55.7812	160.3288	lava	HAB
K01-26	0.8-1.4 ka	Peschanie Gorki cone	55.7223	160.2892	lava	HAB
K01-32	1.4-1.7 ka	1004 cone	55.6725	160.2401	bomb	HAB
K01-55	0.8-1.4 ka	Alaid cone	55.7140	160.2805	lava	HAB
K01-47	<0.8 ka ?	lava field	55.7812	160.3288	bomb	HAB
K01-40	1976 AD	Southern vent	55.5993	160.1850	lava	HAB
Tolb2	11/27/2012	Maiskoe village	56.2280	160.1040	fine ash	HAB
D1311-2	2/26/2013	II cone	55.7620	160.3114	lapilli	HAB
D1314	3/3/2013	lava flow front	55.7500	160.3000	lava	HAB
K01-63	1975 AD	Northern vent, cone 3	55.6965	160.2472	xenolith	HMB
K01-36	1975 AD	Northern vent, cone 2	55.6857	160.2387	xenolith	HAB
K01-27	0.8-1.4 ka	Peschanie Gorki cone	55.7223	160.2892	xenolith	HAB
K01-65	Q_3	Kosirevsk village	56.0460	159.8492	basement lava	HAB

Table 2. Major and trace element analyses of the Tolbachik volcanic field rocks

Sample no.		K01-46B	K01-29	K01-25	K01-46A	K01-30	K01-35	K01-56	K01-57	K01-58	K01-52	K01-54	K01-37	K01-59A	K01-34	K01-59B	K01-49	K01-26	K01-32	K01-55	K01-47
Rock type	Unit	HMB	K-HMB	HMB	HMB	K-HMB	K-HMB	HMB	INTB	INTB	INTB	INTB	INTB	INTB	INTB	HAB	HAB	HAB	HAB	HAB	HAB
SiO_2	wt.%	49.4	50.3	50.9	49.6	50.0	50.6	51.0	51.2	50.8	50.4	50.4	50.6	51.1	51.1	51.3	50.8	51.9	51.7	51.4	51.7
TiO_2	wt.%	1.02	1.25	0.88	1.03	1.28	1.03	0.93	1.15	1.24	1.25	1.15	1.26	1.40	1.34	1.42	1.58	1.61	1.44	1.45	1.47
Al_2O_3	wt.%	13.4	13.3	13.5	13.5	13.4	13.9	13.8	14.5	14.8	14.6	15.1	15.4	15.0	16.1	16.7	16.3	16.2	17.3	17.2	17.2
Fe_2O_{3t}	wt.%	10.56	10.76	9.99	10.56	10.87	10.09	9.96	10.23	10.47	10.21	10.47	10.08	10.98	10.09	10.37	11.06	11.05	10.25	10.35	10.27
MnO	wt.%	0.18	0.17	0.17	0.18	0.17	0.17	0.17	0.17	0.17	0.17	0.17	0.16	0.18	0.16	0.16	0.18	0.18	0.16	0.16	0.16
MgO	wt.%	10.7	10.7	10.6	10.6	10.3	9.88	9.68	8.8	8.66	8.51	8.06	7.56	7.25	6.86	5.66	5.34	4.99	4.99	4.92	4.69
CaO	wt.%	11.4	9.49	11.3	11.4	9.40	10.7	11.3	10.0	9.13	9.75	10.3	9.77	9.15	9.41	8.78	8.84	8.36	8.68	8.56	8.47
Na_2O	wt.%	2.33	2.60	2.31	2.37	2.53	2.62	2.37	2.58	2.82	2.85	2.73	2.92	2.97	3.20	3.22	3.17	3.30	3.43	3.40	3.47
K_2O	wt.%	0.76	1.29	0.72	0.77	1.27	1.01	0.78	1.17	1.33	1.34	1.15	1.39	1.49	1.54	1.57	1.75	1.92	1.71	1.72	1.75
P_2O_5	wt.%	0.20	0.33	0.18	0.20	0.36	0.26	0.20	0.33	0.38	0.38	0.31	0.38	0.43	0.43	0.45	0.54	0.57	0.47	0.47	0.49
H_2O	wt.%	0.27	0.28	0.16	0.23	0.56	0.18	0.13	0.17	0.20	0.22	0.34	0.21	0.28	0.23	0.21	0.20	0.10	0.23	0.18	0.26
CO_2	wt.%	0.03	0.03	0.02	0.02	0.05	0.02	0.02	0.02	0.03	0.02	0.03	0.03	0.03	0.03	0.01	0.01	0.02	0.02	0.03	0.03
Sum	wt.%	100.2	100.5	100.7	100.5	100.2	100.4	100.3	100.3	100.0	99.7	100.1	99.7	100.3	100.5	99.9	99.7	100.1	100.4	99.8	100.0
Co	ppm	48	46	44	48	46	43	43	42	42	41	42	40	41	37	36	38	36	35	36	34
Cr *	ppm	507.2	620.6	487.0	473.7	589.5	420.1	401.0	460.2	435.5	430.6	310.1	281.1	237.0	251.2	95.8	89.1	66.4	55.2	50.0	48.3
2σ	ppm	(4.5)	(1.5)	(1.6)	(1.4)	(3.9)	(4.7)	(4.3)	(1.8)	(4.6)	(4.0)	(2.9)	(2.0)	(2.0)	(2.0)	(2.2)	(1.3)	(2.4)	(0.9)	(1.3)	(0.7)
Ni *	ppm	139.1	184.0	135.0	127.1	167.5	129.9	109.3	126.5	140.0	128.0	92.5	91.3	83.8	85.3	49.3	32.9	29.9	43.1	42.0	39.2
2σ	ppm	(0.7)	(1.2)	(0.4)	(0.6)	(0.7)	(0.6)	(0.6)	(1.0)	(0.6)	(0.4)	(0.4)	(0.7)	(0.7)	(0.6)	(0.6)	(0.4)	(0.9)	(0.9)	(0.4)	(0.6)
V *	ppm	292.4	294.2	283.4	291.4	303.1	267	279.2	288	281.8	279.7	297.9	283.9	299.1	285.9	252.9	280.5	270.8	291.5	287.4	300.6
2σ	ppm	(2.6)	(1.3)	(2.0)	(2.2)	(2.1)	(1.5)	(3.2)	(2.0)	(2.6)	(2.5)	(2.2)	(2.3)	(1.1)	(2.2)	(1.9)	(3.0)	(1.8)	(0.9)	(1.9)	(2.4)
Zn *	ppm	79.6	86.1	73.9	78.5	85.5	75.6	73.8	83.4	87.2	86.6	83.4	85.9	95.1	90.6	79.3	84	86.8	92.1	95.2	94.4
2σ	ppm	(0.8)	(0.8)	(1.0)	(0.7)	(1.0)	(0.7)	(0.5)	(1.0)	(0.5)	(1.0)	(0.6)	(1.1)	(0.5)	(0.5)	(1.1)	(0.9)	(0.6)	(1.5)	(0.8)	(0.7)
La *	ppm	5.8	10.2	6.0	5.3	10.8	8.2	6.3	10.7	10.9	10.7	8.8	10.1	12.5	12.6	13.6	14.5	15.9	14.4	15.2	14.3
2σ	ppm	(0.9)	(1.3)	(1.0)	(0.8)	(0.3)	(0.8)	(0.9)	(0.8)	(1.1)	(0.9)	(0.6)	(1.0)	(0.8)	(1.0)	(0.7)	(1.0)	(0.8)	(0.9)	(1.2)	(0.9)
Ce *	ppm	18.3	27.8	14.6	18	28.8	18.3	14.4	25.4	30.5	31.7	26	27.8	35.4	31.8	34.1	40.6	41.6	36.8	37.5	37.5
2σ	ppm	(2.1)	(1.6)	(2.5)	(1.3)	(2.2)	(3.3)	(2.3)	(2.4)	(2.3)	(2.0)	(1.6)	(1.4)	(1.7)	(1.9)	(2.3)	(1.8)	(1.6)	(2.8)	(2.2)	(3.0)
Nd *	ppm	14.3	20.2	12.2	14.8	20.3	15.4	12	18.1	20.1	21.2	17.8	18.8	23.6	22.4	23.4	27.3	26.9	24	25	24.8
2σ	ppm	(1.0)	(1.0)	(1.3)	(0.9)	(1.4)	(1.3)	(1.5)	(1.0)	(1.2)	(1.3)	(1.0)	(0.6)	(0.7)	(1.0)	(1.0)	(1.1)	(0.8)	(1.0)	(1.0)	(1.4)
Nb *	ppm	1.0	2.3	1.3	0.9	2.6	1.7	1.2	2.5	3.1	2.8	2.1	3.0	3.6	3.5	3.7	4.0	4.9	3.8	3.9	4.1
2σ	ppm	(0.3)	(0.2)	(0.2)	(0.2)	(0.2)	(0.2)	(0.1)	(0.2)	(0.2)	(0.1)	(0.1)	(0.2)	(0.2)	(0.2)	(0.2)	(0.2)	(0.1)	(0.1)	(0.1)	(0.1)
Ga *	ppm	13.7	14.7	13.7	13.6	15.0	14.0	14.1	16.7	16.4	15.5	15.6	15.5	17.5	17.4	18.3	16.4	18.7	17.4	17.3	18.3
2σ	ppm	(1.1)	(0.7)	(0.9)	(1.2)	(1.1)	(0.9)	(0.6)	(0.8)	(0.5)	(0.5)	(0.8)	(1.0)	(0.7)	(0.8)	(1.0)	(1.0)	(0.9)	(1.1)	(0.9)	(0.9)
Pb *	ppm	1.1	2.7	1.7	1.0	5.2	1.6	1.9	3.0	3.1	2.7	2.1	3.0	3.9	3.2	3.9	3.7	4.7	3.7	3.8	4.2
2σ	ppm	(0.5)	(0.4)	(0.5)	(0.6)	(0.5)	(0.2)	(0.4)	(0.5)	(0.5)	(0.6)	(0.8)	(0.4)	(0.4)	(0.6)	(0.4)	(0.5)	(0.4)	(0.4)	(0.5)	(0.6)
Rb *	ppm	14.1	30.9	14.2	14.4	31.0	20.5	15.7	27.9	32.5	30.0	26.0	31.4	36.9	35.5	39.3	44.9	49.1	40.7	41.8	42.6
2σ	ppm	(0.3)	(0.3)	(0.4)	(0.6)	(0.5)	(0.3)	(0.5)	(0.6)	(0.2)	(0.4)	(0.4)	(0.3)	(0.4)	(0.3)	(0.4)	(0.2)	(0.6)	(0.5)	(0.6)	(0.4)
Ba *	ppm	195.0	311.5	219.7	202.3	315.0	253.5	234.6	311.5	335.3	316.1	289.6	327.0	374.1	371.4	412.5	407.2	483.6	421.0	417.0	425.9
2σ	ppm	(3.3)	(3.4)	(2.1)	(2.5)	(4.2)	(1.9)	(4.2)	(3.3)	(2.2)	(3.1)	(4.7)	(2.9)	(3.9)	(4.1)	(4.9)	(3.7)	(3.1)	(3.7)	(4.7)	(5.9)

Sr *	ppm	252.0	287.7	270.9	249.1	278.7	269.5	275.4	290.0	296.2	284.4	313.4	298.9	295.4	316.2	348.7	330.1	319.5	354.3	354.4	354.2
2σ	ppm	(0.5)	(1.6)	(0.7)	(2.0)	(1.1)	(0.5)	(0.5)	(0.9)	(1.2)	(0.5)	(1.8)	(2.3)	(0.7)	(0.4)	(0.9)	(0.9)	(0.9)	(1.6)	(1.4)	(0.9)
Th *	ppm	0.2	1.0	0.7	0.8	1.0	0.6	0.4	1.2	1.4	0.9	1.0	1.6	1.5	1.8	1.7	1.4	1.8	1.5	1.8	1.7
2σ	ppm	(0.4)	(0.3)	(0.3)	(0.4)	(0.4)	(0.3)	(0.4)	(0.4)	(0.4)	(0.3)	(0.3)	(0.4)	(0.2)	(0.4)	(0.2)	(0.3)	(0.4)	(0.4)	(0.3)	(0.6)
Y *	ppm	20.8	25.3	18.9	21.0	25.4	20.6	19.9	25.2	26.5	25.0	24.4	25.5	30.6	27.5	30.4	33.9	35.8	29.6	30.7	31.5
2σ	ppm	(0.3)	(0.4)	(0.2)	(0.4)	(0.3)	(0.5)	(0.5)	(0.2)	(0.6)	(0.3)	(0.4)	(0.4)	(0.4)	(0.3)	(0.3)	(0.3)	(0.3)	(0.5)	(0.5)	(0.5)
Zr *	ppm	71.6	123.5	72.5	71.9	124.6	91.5	78.3	121.9	138.4	132.7	111.5	134.2	160.6	151.4	162.4	173.0	198.2	167.4	168.3	173.1
2σ	ppm	(0.5)	(0.4)	(1.2)	(0.5)	(0.7)	(0.3)	(0.8)	(0.8)	(0.7)	(0.7)	(0.7)	(0.4)	(0.8)	(0.3)	(0.7)	(1.7)	(0.6)	(0.5)	(0.7)	(0.7)
Sc *	ppm	41.5	36.5	42.8	39.6	37.4	36.2	41.1	38.5	34.2	33.1	38.0	34.3	34.4	31.5	26.2	27.9	27.3	26.4	26.6	27.3
2σ	ppm	(1.5)	(1.0)	(1.2)	(1.3)	(0.7)	(0.9)	(0.5)	(0.8)	(1.0)	(0.4)	(0.9)	(0.6)	(0.7)	(0.6)	(0.9)	(0.9)	(0.5)	(0.7)	(0.6)	(1.2)
Cu *	ppm	104.1	128.8	144.9	107.0	131.8	131.6	103.5	119.6	159.1	164.6	105.0	165.9	209.3	181.4	147.6	148.9	123.5	192.7	193.9	182.8
2σ	ppm	(0.6)	(0.6)	(0.9)	(1.0)	(0.9)	(0.5)	(0.6)	(0.8)	(0.5)	(1.4)	(1.1)	(1.0)	(1.0)	(0.7)	(0.6)	(0.8)	(1.2)	(0.6)	(1.2)	(1.1)
Cl *	ppm	335.1	326.7	293.2	328.9	263.6	426.3	403.8	238.4	44.4	332.4	249.7	293.6	124.1	324.9	137.9	403.6	99.7	150.7	181.1	261.0
2σ	ppm	(12.8)	(8.6)	(11.4)	(8.6)	(17.2)	(16.2)	(21.6)	(20.8)	(18.7)	(13.2)	(14.5)	(11.1)	(28.5)	(9.7)	(9.2)	(12.2)	(8.4)	(11.2)	(13.8)	(16.5)

Notes: Data marked with asterisk are high-precision XRF data measured at RHUL (reported with 2σ).

Data on reference samples analyzed in one series with Tolbachik rocks are reported in supplementary Table A1.

Table 2. continued

Sample no.		K01-40	Tolb2	D1311-2	D1314	K01-63	K01-36	K01-27	K01-65
Rock type	Unit	HAB	HABA	HAB	HAB	xenolith	xenolith	xenolith	basement
SiO_2	wt.%	51.6	54.85	51.8	51.6	51.2	53.2	53.5	53.6
TiO_2	wt.%	1.65	2.12	1.99	1.97	1.08	1.18	1.07	1.62
Al_2O_3	wt.%	17.2	15.11	16.0	16.0	14.4	18.6	16.6	16.9
Fe_2O_{3t}	wt.%	10.51	10.86	11.72	11.67	9.67	8.23	9.23	9.66
MnO	wt.%	0.16	0.20	0.18	0.18	0.15	0.12	0.17	0.15
MgO	wt.%	4.59	3.21	4.13	4.08	9.32	3.75	5.72	3.51
CaO	wt.%	8.06	6.61	7.37	7.43	8.38	8.12	8.60	7.27
Na_2O	wt.%	3.56	3.94	3.41	3.44	3.09	3.82	3.23	3.82
K_2O	wt.%	2.03	3.13	2.41	2.43	1.45	2.12	1.33	2.07
P_2O_5	wt.%	0.59	0.83	0.74	0.73	0.30	0.46	0.26	0.54
H_2O	wt.%	0.16				0.14	0.24	0.17	0.49
CO_2	wt.%	0.01				0.02	0.02	0.02	0.03
Sum	wt.%	100.1	100.9	99.8	99.5	99.2	99.8	99.9	99.6
Co	ppm	34		27	29	40	27	33	29
Cr *	ppm	67.3		34	33	431.5	80.1	70.1	35.2
2 s.d.	ppm	(1.1)				(3.0)	(2.0)	(0.9)	(0.9)
Ni *	ppm	41.1		40.0	46.0	151.2	43.5	34.9	29.0
2 s.d.	ppm	(0.7)				(0.6)	(0.4)	(0.3)	(0.8)
V *	ppm	278.3		315	314	249.3	265.7	251.8	312.7
2 s.d.	ppm	(2.2)				(2.2)	(1.1)	(1.4)	(2.0)
Zn *	ppm	91.9		119	117	79.9	79	78.3	93.1
2 s.d.	ppm	(0.7)				(0.7)	(0.9)	(0.9)	(0.9)

La *	ppm	16.8			10.8	14.2	9.6	17
2 s.d.	ppm	(0.5)			(0.9)	(1.2)	(0.8)	(0.7)
Ce *	ppm	42.6			25	32	21.9	40.5
2 s.d.	ppm	(2.5)			(2.4)	(2.1)	(1.1)	(2.5)
Nd *	ppm	26.2			17.3	22.4	16.3	28.7
2 s.d.	ppm	(1.4)			(1.1)	(1.0)	(0.8)	(1.2)
Nb *	ppm	5.0	8	9	2.3	3.5	2.1	4.0
2 s.d.	ppm	(0.3)			(0.1)	(0.2)	(0.1)	(0.2)
Ga *	ppm	18.1	25	24	17.1	20.7	18.2	18.6
2 s.d.	ppm	(0.7)			(0.7)	(1.0)	(1.2)	(0.8)
Pb *	ppm	3.5			3.9	5.9	3.8	6.6
2 s.d.	ppm	(0.3)			(0.5)	(0.5)	(0.5)	(0.5)
Rb *	ppm	49.0	59	60	25.0	43.2	24.9	41.4
2 s.d.	ppm	(0.4)			(0.1)	(0.4)	(0.3)	(0.2)
Ba *	ppm	486.1	566	553	464.0	731.1	491.2	621.8
2 s.d.	ppm	(3.0)			(4.7)	(5.4)	(3.9)	(4.0)
Sr *	ppm	325.7	311	315	355.0	538.2	408.1	364.2
2 s.d.	ppm	(0.7)			(0.9)	(1.3)	(1.0)	(0.7)
Th *	ppm	1.8			1.0	2.3	1.7	1.8
2 s.d.	ppm	(0.4)			(0.3)	(0.3)	(0.4)	(0.2)
Y *	ppm	33.6	43	43	19.9	26.2	24.6	35.4
2 s.d.	ppm	(0.3)			(0.6)	(0.4)	(0.4)	(0.4)
Zr *	ppm	201.7	262	259	115.3	154.4	111.4	214.6
2 s.d.	ppm	(0.7)			(0.5)	(0.7)	(0.5)	(0.8)
Sc *	ppm	24.9	30	21	25.0	19.9	32.2	24.4
2 s.d.	ppm	(1.2)			(0.6)	(0.5)	(0.6)	(0.9)
Cu *	ppm	198.0	266	200	124.8	150.2	56.3	233.5
2 s.d.	ppm	(1.0)			(1.0)	(0.9)	(0.6)	(1.2)
Cl *	ppm	47.9			38.0	224.3	42.9	150.2
2 s.d.	ppm	(20.2)			(14.0)	(14.4)	(7.4)	(24.2)

Table 3. Representative ICP-MS analyses of rocks from the Tolbachik volcanic field

		1	2	3	4	5	6	7	8
Sample no.		K01-25	K01-30	K01-54	22-8			*Variability*	D_i
Age/Year		0.8-1.4 ka	1.4-1.7 ka	0.8-1.7 ka	1976	2012	2013		
Rock type	Unit	HMB	K-HMB	INTB	HAB	HAB	HAB		
MgO	wt.%	10.6	10.3	8.1	4.3	4.1	3.2	*0.49*	
TiO_2	wt.%	0.88	1.28	1.15	1.59	1.95	1.76	*0.28*	*0.134*
K_2O	wt.%	0.72	1.27	1.15	1.97	2.39	2.55	*0.44*	*0.065*
Li	ppm	7.14	8.26	8.74	14.7	18.6	21.3	*0.45*	
Sc	ppm	43.2	36.5	37.3	22.0	28.3	26.6	*0.25*	
V	ppm	361	394	385	270	290	239	*0.20*	
Cr	ppm	513	400	306	165	37	12	*0.84*	
Co	ppm	44.6	45.5	40.8	30.0	32.0	25.0	*0.23*	
Ni	ppm	146	181	97	45	41	11	*0.76*	
Cu	ppm	151	143	116					
Zn	ppm	76.0	91.3	86.9	99.0				
Ga	ppm	15.4	17.6	17.8	19.0	20.9	20.6	*0.11*	
Rb	ppm	14.5	33.8	27.5	52.0	60.7	64.5	*0.47*	*0.025*
Sr	ppm	292	320	342	362	303	317	*0.08*	*0.680*
Y	ppm	19.1	27.1	24.8	32.0	45.0	51.0	*0.37*	
Zr	ppm	66.9	122	105	199	243	260	*0.48*	*0.054*
Nb	ppm	1.51	3.02	2.54	5.16	8.11	8.93	*0.63*	*0.010*
Mo	ppm	0.49	0.97	0.82					
Sn	ppm	0.82	2.69	1.08					
Sb	ppm	0.08	0.16	0.13					
Cs	ppm	0.45	0.85	0.81	1.58	2.28	2.50	*0.60*	
Ba	ppm	196	290	267	467	551	588	*0.42*	*0.180*
La	ppm	6.07	11.2	9.66	17.0	21.3	23.0	*0.46*	*0.048*
Ce	ppm	15.4	27.9	24.3	41.9	55.4	60.1	*0.48*	*0.065*
Pr	ppm	2.40	4.30	3.73	6.42	7.48	8.00	*0.42*	
Nd	ppm	11.6	19.9	17.5	29.0	34.3	36.7	*0.40*	*0.118*

Sm	ppm	3.14	5.01	4.54	7.14	8.23	8.70	*0.36*	*0.179*
Eu	ppm	0.98	1.41	1.31	1.84	2.15	2.30	*0.31*	*0.208*
Gd	ppm	3.25	4.88	4.46	6.22	8.18	8.80	*0.37*	*0.226*
Tb	ppm	0.54	0.78	0.72	0.97	1.23	1.35	*0.34*	
Dy	ppm	3.35	4.69	4.31	5.66	7.30	7.85	*0.32*	*0.253*
Ho	ppm	0.68	0.94	0.87	1.17	1.50	1.65	*0.33*	
Er	ppm	1.88	2.63	2.43	3.47	4.45	4.70	*0.35*	*0.254*
Tm	ppm	0.27	0.38	0.35	0.49	0.60	0.70	*0.35*	
Yb	ppm	1.79	2.49	2.34	3.19	4.07	4.45	*0.34*	*0.242*
Lu	ppm	0.27	0.37	0.34	0.52	0.60	0.70	*0.36*	*0.231*
Hf	ppm	1.90	3.20	2.81	5.21	6.60	7.30	*0.49*	
Ta	ppm	0.09	0.18	0.15	0.36	0.50	0.55	*0.63*	
W	ppm	0.08	0.16	0.14					
Tl	ppm	0.04	0.16	0.07	0.05	0.13	0.10	*0.52*	
Pb	ppm	2.06	5.26	2.71	7.49	8.18	9.05	*0.51*	
Th	ppm	0.63	1.20	1.05	2.31	2.77	3.45	*0.58*	
U	ppm	0.35	0.67	0.60	1.26	1.97	2.05	*0.64*	

Notes: Major elements (in wt.%) - XRF data, trace elements (in ppm) - ICP-MS data.
1-3 - this study; 4 - Churikova et al. (2001); 5-6 - average compositions from Volynets et al. (2014); 7 - trace element variability calculated as 1σ/Cmean; 8 - bulk partition coefficients. D_i for K, Rb, Ba, Nb are calculated from D_j for plagioclase from Bindeman et al. (1998) assuming 50% plagioclase on cotectics and D_i olivine and pyroxene equal to 0; D_i for other elements are from compilation of O'Neill and Jenner (2012) for global MORB. Data on reference samples analyzed in one series with Tolbachik rocks are

Table 4. Sr-Nd-Pb and O isotope data for Tolbachik rocks

Sample no.	Rock type	Lab	$^{87}Sr/^{86}Sr$	2SE	$^{143}Nd/^{144}Nd$	2SE	$^{206}Pb/^{204}Pb$	2SE	$^{207}Pb/^{204}Pb$	2SE	$^{208}Pb/^{204}Pb$	2SE	$\delta^{18}O_{SMOW}$	Phase analyzed
				ppm		ppm	DS		DS		DS			
K01-29	K-HMB	RHUL	0.703393	(13)	0.513082	(4)	18.2039	(0.0012)	15.4755	######	37.8693	(0.0029)		
K01-29 dupl.	K-HMB	RHUL			0.513087	4								
K01-25	HMB	RHUL	0.703316	(11)	0.513086	(4)	18.1994	(0.0011)	15.4732	######	37.8661	(0.0029)	5.56	Ol
K01-25 dupl.	HMB	RHUL			0.513091	(5)								
K01-46A	HMB	RHUL	0.703335	(10)	0.513084	(4)								
K01-46A dupl.	HMB	RHUL			0.513086	(5)								
K01-30	K-HMB	RHUL	0.703399	(9)	0.513080	(4)	18.2031	(0.0011)	15.4749	######	37.8690	(0.0028)	5.61	Ol
K01-35	K-HMB	RHUL	0.703358	(9)	0.513074	(5)								
K01-56	HMB	RHUL	0.703336	(9)	0.513076	(12)								
K01-57	INTB	RHUL	0.703351	(10)										
K01-58	INTB	RHUL	0.703364	(13)	0.513080	(5)	18.1904	(0.0009)	15.4740	######	37.8632	(0.0022)	5.37	Ol
K01-52	INTB	RHUL	0.703356	(9)			18.1818	(0.0016)	15.4733	######	37.8507	(0.0042)	5.56	Ol
K01-54	INTB	RHUL	0.703357	(9)	0.513073	(4)	18.1892	(0.0010)	15.4742	######	37.8591	(0.0027)	5.60	Ol
K01-37	INTB	RHUL	0.703359	(10)										
K01-59A	INTB	RHUL	0.703351	(11)	0.513089	(5)								
K01-34	INTB	RHUL	0.703366	(12)	0.513076	(5)								
K01-59B	HAB	RHUL	0.703333	(9)										
K01-49	HAB	RHUL	0.703247	(11)	0.513088	(4)	18.1733	(0.0012)	15.4704	######	37.8364	(0.0031)	5.38	Ol
K01-26	HAB	RHUL	0.703421	(10)	0.513081	(6)	18.1791	(0.0012)	15.4710	######	37.8477	(0.0033)		
K01-32	HAB	RHUL	0.703362	(10)	0.513086	(5)	18.1895	(0.0007)	15.4744	######	37.8625	(0.0018)		
K01-32 dupl.	HAB	RHUL	0.703362	(12)										
K01-40	HAB	RHUL	0.703385	(11)	0.513089	(5)	18.1853	(0.0013)	15.4741	######	37.8617	(0.0037)	6.05	Ol
K01-40 dupl.	HAB	RHUL			0.513086	(8)								
Tolb2	HAB	GEOMAR	0.703376	(4)	0.513093	(4)	18.1882	(0.0006)	15.4753	######	37.8651	(0.0015)	6.16	Glass

D1314	HAB	GEOMAR	0.703379	(4)	0.513081	(6)	18.1826	(0.0006)	15.4728	######	37.8543	(0.0020)	6.13	Glass
D1314	HAB	GEOMAR											6.31	Pl
D1306	HAB	GEOMAR											6.16, 6.04	Glass
K01-36	Xenolith	RHUL	0.703514	(10)	0.513076	(4)								
K01-27	Xenolith	RHUL	0.703560	(12)	0.513063	(4)								
K01-65	Basement	RHUL	0.703534	(21)	0.513089	(9)								

Notes: Sr, Nd and Pb isotope data were obtained at RHUL and GEOMAR, O isotope data - at the University of Oregon. Phase analyzed is indicated for the O-isotope data.

Table 5. Primary magmas of Tolbachik and other CKD volcanoes calculated in PRIMACALC2.

		Volcano			
	Unit	Tolbachik	Klyuchevskoy	Shiveluch	Shisheisky
Primitive rocks					
SiO_2	wt.%	50.7	52.8	54.1	56.4
TiO_2	wt.%	0.97	0.89	0.79	0.70
Al_2O_3	wt.%	13.7	15.1	14.9	15.4
FeO	wt.%	9.5	8.6	7.7	6.5
MnO	wt.%	0.17	0.17	0.15	0.12
MgO	wt.%	10.2	9.1	9.4	8.6
CaO	wt.%	11.2	9.6	8.3	6.7
Na_2O	wt.%	2.4	2.8	3.0	4.2
K_2O	wt.%	0.82	0.81	1.34	1.14
P_2O_5	wt.%	0.21	0.16	0.27	0.17
Total	wt.%	100.0	100.0	100.0	99.9
Ni	ppm	128	116	109	170
Model primary melts					
SiO_2	wt.%	49.7	51.2	52.7	54.6
TiO_2	wt.%	0.88	0.78	0.71	0.62
Al_2O_3	wt.%	12.4	13.2	13.4	13.6

FeO	wt.%		9.7		8.9	8.0	6.9
MnO	wt.%		0.17		0.17	0.14	0.12
MgO	wt.%		13.9		14.0	13.5	13.4
CaO	wt.%		10.1		8.4	7.4	5.9
Na_2O	wt.%		2.2		2.4	2.7	3.7
K_2O	wt.%		0.74		0.71	1.21	1.01
P_2O_5	wt.%		0.19		0.14	0.24	0.15
Total	wt.%		100.0		100.0	100.0	100.0
H_2O	wt.%	2.8	4.0	6.0	4.0	4.0	4.0
Ni	ppm	321	353	426	585	335	704
Olivine NiO	wt.%	0.29	0.37	0.53	0.62	0.35	0.71
Olivine Fo	mol.%	91.1	91.0	90.9	91.5	92.2	93.1
Mg# melt		0.72	0.72	0.72	0.74	0.75	0.78
T	^oC	1344	1291	1247	1254	1239	1224
P	GPa	1.8	1.8	1.8	1.2	1.0	0.8
F	wt.%	22	20	20	25	26	27
X_{frac}	mol.%	13	12	12	16	13	15

Notes: Primitive rocks compositions: Tolbachik - average medium-K HMB from this study, Klyuchevskoy, Shiveluch and Shisheisky - after Portnyagin et al. (2007). Major element oxides are in wt.%. Primary melt compositions were calculated in PRIMACALC2.0 program (Kimura and Ariskin, 2014).
T - wet mantle temperature, P - pressure , F - degree of melting, X_{frac} - degree of crystal fractionation from primary melt to primitive rock composition. NiO in olivine was calculated using model of Li and Ripley (2010).

Table 6. Trace element and isotope composition of primary Tolbachik melt, source components and results of best-fit ABS3 calculations

	Input compositions					ABS3 calculated compositions				
Element	Tolbachik primary melt	KMW	NWPS	MORB AOC	Meiji AOC	NWPS melt	MORB-AOC melt	Meiji-AOC melt	Composite slab melt	Tolbachik calculated melt
Rb	13.0	0.088	54	7.5	19	9	13	32	18.5	9.5
Ba	176	1.20	1560	30	83	4451	60	166	310	156
Th	0.56	0.014	3.8	0.12	0.63	5.73	0.33	1.74	1.00	0.59
U	0.31	0.005	2.0	0.08	0.84	2.35	0.11	1.17	0.52	0.29
Nb	1.35	0.21	5.5	1.98	9.6	0.43	0.10	0.46	0.22	1.9
Ta	0.08	0.014	0.36	0.12	0.61	0.029	0.006	0.029	0.013	0.13
K	5357	60	19090	3265	16040	3339	5747	28234	12035	6146
La	5.45	0.23	15.2	2.9	9.1	11.2	6.0	19.0	10.0	6.6
Ce	13.8	0.77	31	9.8	23.7	25.9	21.9	53.1	31.0	20.4
Pb	1.85	0.023	11.0	0.24	0.9	23.9	0.6	2.4	2.3	1.2
Pr	2.15	0.13	*4.0*	1.80	3.5	2.6	2.4	4.6	3.0	2.4
Sr	262	9.8	265	153	218	480	521	745	583	325
Nd	10.4	0.71	18.1	9.8	16.0	9.2	8.9	14.5	10.5	10.1
Sm	2.82	0.27	4.1	3.4	4.6	1.2	1.0	1.4	1.1	2.6
Zr	60	7.9	92	100	135	25	19	26	21	67
Hf	1.70	0.20	2.3	2.4	3.5	0.64	0.49	0.71	0.56	1.6
Eu	0.88	0.11	1.0	1.2	1.6	0.24	0.26	0.34	0.28	0.9
Gd	2.91	0.40	*3.5*	4.5	5.3	0.53	0.52	0.62	0.55	3.0
Tb	0.48	0.08	0.7	0.8	0.9	0.07	0.06	0.06	0.06	0.5
Dy	3.01	0.53	*4.0*	5.5	5.8	0.30	0.26	0.27	0.27	3.1
Y	17.1	3.26	24	36	29.7	1.30	1.14	0.95	1.1	17.6
Ho	0.61	0.12	*0.85*	1.2	1.2	0.05	0.04	0.04	0.04	0.7
Er	1.69	0.37	*2.50*	3.3	3.4	0.11	0.10	0.11	0.11	1.9
Tm	0.24	0.06	*0.35*	0.5	0.5	0.01	0.01	0.01	0.01	0.3
Yb	1.61	0.40	2.3	3.3	3.1	0.07	0.07	0.06	0.07	1.6
Lu	0.24	0.06	0.3	0.5	0.5	0.01	0.01	0.01	0.01	0.3

$^{87}Sr/^{86}Sr$	0.70343	0.70281	0.70650	0.70325	0.70319	0.70650	0.70325	0.70319	0.70336	0.70323
$^{143}Nd/^{144}Nd$	0.51310	0.51310	0.51260	0.51320	0.51304	0.51260	0.51320	0.51304	0.51311	0.51310
$^{206}Pb/^{204}Pb$	18.2	17.8	18.6	18.2	18.9	18.6	18.2	18.9	18.6	18.5
$^{207}Pb/^{204}Pb$	15.5	15.4	15.6	15.4	15.5	15.6	15.4	15.5	15.5	15.5
$^{208}Pb/^{204}Pb$	37.9	37.7	38.6	37.5	38.0	38.6	37.5	38.0	38.2	38.1

Notes. Tolbachik primary melt was calculated in PRIMACALC2 from HMB sample K01-25; NKMW - North Kamchatka mantle wedge: trace elements - DMM after Salters and Stracke (2004), isotope ratios - after Portnyagn et al. (2005); NWPS - North-West Pacific sediments (Bailey, 1995; Bindeman et al., 2004). Values for Pr, Gd, Dy, Ho, Er, Tm were interpolated from the neighbouring REE; MORB-AOC - average MORB from Kamchatka ophiolite (Duggen et al., 2007); MEIJI-AOC - average Meiji basalt from DSDP Site 192 (Regelous et al., 2003; Keller et al., 2000).

Calculated ABS3 compositions: MORB-AOC, MEIJI-AOC, NWPS melts are water-bearing slab melts from pure end-member lithologies. Composite slab melt is comprised by 5% NWPS melt, 27.5% Meiji-AOC melt, and 67.7% MORB-AOC melts. All slab melt compositions were calculated for 725 °C and 2.8 GPa.

Calculated Tolbachik primary melt corresponds to mantle peridotite melt produced at 2 GPa, 1250 °C by 6.4% melting of NKMW source with addition of 7% of COMP fluid.